SURFER ~~v1~~v2.0: A flexible and simple model linking emissions to ocean acidification and sea level rise

Marina Martínez Montero[1], Michel Crucifix[1], Victor Couplet[1], Nuria Brede[2,4], and Nicola Botta[2,3]

[1]Earth and Life Institute, UCLouvain, Louvain-la-Neuve, Belgium
[2]Potsdam Institute for Climate Impact Research, Potsdam, Germany
[3]Chalmers University of Technology, Göteborg, Sweden
[4]University of Potsdam, Potsdam, Germany

Correspondence: Marina Martínez Montero (marina.martinez@uclouvain.be)

Abstract. We present SURFER, a ~~model for~~ novel reduced model for estimating the impact of CO_2 emissions and solar radiation management options on sea level rise ~~that consists of three sub-models: an updated and expanded version of BEAM carbon cycle model (Glotter et al., 2014), a 2-box climate model that allows for~~ and ocean acidification over timescales of several thousands of years. SURFER has been designed for the analysis of CO_2 emission and solar radiation management policies, for supporting the computation of optimal (CO_2 emission and solar radiation management~~and a simple ice sheet model that represents the tipping points and related timescales of Greenland and Antarctic ice sheets. The model, consisting of 8~~) policies and for the study of commitment and responsibility under uncertainty. The model is based on a combination of conservation laws for the masses of atmospheric and oceanic carbon and for the oceanic temperature anomalies, and of ad-hoc parametrisations for the different sea level rise contributors: ice sheets, glaciers and ocean thermal expansion. It consists of 9 loosely coupled ordinary differential equations, is ~~fast, accurate up to timescales of several thousands of years and has been calibrated to reproduce results obtained by state of the art carbon cycle and ice sheet models. Additionally the ice sheet sub-model has been written in a flexible way that allows easily updating its parameters to match future results~~ understandable, fast and easy to modify and calibrate. It reproduces the results of more sophisticated, high-dimensional earth system models on time scales up to millennia.

1 Introduction

~~Policy analysis and policy advice in the field of climate change is challenging and complex. Not only is it important to take into account up to date knowledge in climate science, but it is also important to be transparent and fair in the priorities and values that go into obtaining results used for advice.~~ Carbon emissions in the following decades will have a significant impact on the sea level and on the acidity of the oceans for millennia (e.g., Clark et al., 2016; Van Breedam et al., 2020), mainly because the long residence time of CO_2 in the atmosphere-ocean system (Archer, 2005; Archer et al., 2009).

~~A classical approach to policy advice is that of cost-benefit analysis where one proceeds by minimising a cost function — equivalently, maximising a utility function — such as to determine an optimal carbon tax, or answer questions like "what is the optimal way/path of reducing greenhouse gases (GHG) emissions in the next 100 years". There has been a rising (but criticised,~~

see (Gardiner, 2010)) interest for addressing the trade-offs associated with geoengineering mitigation options, such as to determine the “optimal mix of geoengineering and GHG emission reduction" (e.g., Moreno-Cruz and Keith, 2013; Helwegen et al., 2019) . In that context, the “utility" is typically an aggregated quantity that somehow measures the world’s welfare[1], taking into account the costs of the different mitigation choices and the costs of Therefore, assessing the value of CO_2 emission policies for the next decades on sea level rise and ocean acidification necessarily has to account for impacts (e.g., in terms of benefits and damages due to climate change during the considered time-framesea level rise and crossing planetary boundaries (Rockström et al., 2009; St) and perhaps solar radiation management costs) over much longer time scales than the next decades.

Most policy analyses put their focus on timescales of several decades to a couple of hundreds of years either by only looking at those timescales or by heavily discounting the future (e.g., Nordhaus, 1992; Moreno-Cruz and Keith, 2013; Helwegen et al., 2019; Hänse , meaning that cost-benefit analyses are only performed taking into consideration the “close” future. Additionally, the considered climate change damages are in general much lower than they should be , see (Keen, 2020; Keen et al., 2021) for an extensive critique. This is partly because only the damages from rising temperatures are considered, ignoring damages from ocean acidification, Failing to do so may lead to short sighted policies that commit upcoming generations to unmanageable impacts or that severely shrinks their range of viable CO_2 emission and/or solar radiation management options (Clark et al., 2016; Mengel et al., 2018; .

Assessing the value of CO_2 emission policies for the next decades over millennia requires accounting for epistemic (Shepherd et al., 2018 model uncertainties but also, and perhaps more importantly, for uncertainties about how these policies will actually be implemented: we know that decisions in matter of greenhouse gas abatements may be implemented with delays and that solar radiation management options for mitigating the impacts of high CO_2 concentrations in the atmosphere are not free from risks, see (Gardiner, 2010; Moreno-Cruz and Keith, 2013; Robock, 2016, 2020; Helwegen et al., 2019). Also, assessing the value of CO_2 emission policies for the next decades based on sea level rise and tipping points among others, and partly because of serious flaws present in the process of estimating the damages due to global warming. ocean acidification necessarily has to account for uncertainties about the (anthropogenic) forcings to be expected after, say, 2100.

It is disturbing that these studies focus on short-term periods given the well-known long residence time of carbon dioxide in the atmosphere-ocean system (Archer, 2005; Archer et al., 2009). Decisions about greenhouse gas emissions in the following decades to hundred years can have the potentially catastrophic consequences for climate and , in particular, sea level rise in the next thousands of years (e.g., Clark et al., 2016; Van Breedam et al., 2020). It is thus necessary to verify that optimal policiesobtained with short-sighted analyses do not commit future generations to undesirable or even unmanageable situations.It would be even better to include such long-term effects in the policy analyses themselvesDepending on the methodology applied and on the level of guarantees (correctness) required, computing “best” climate policies under uncertainty and estimating measures of responsibility for specific climate decisions (Botta et al., 2021) can be more or less computationally expensive than assessing the value of a given policy under the same uncertainties. As a consequence, in presence of uncertainty, various interesting assessments require models that are easy to understand and modify, and fast to apply. Such assessments include

[1] Not all studies maximise a single aggregated welfare quantity. In (Carlino et al., 2020), for example, the authors give optimal multi-objective policies with a time horizon of 500 years.

(among others) the analysis of CO_2 emission policies, the computation of optimal policies, the assessment of commitment, responsibility and safe operating spaces (Heitzig et al., 2016), e.g., in terms of planetary boundaries (Rockström et al., 2009).

State-of-the-art climate models are computationally too expensive to be used in policy analyses that explore many policy or control options, this is one reason why such analyses tend to rely on simplified models. Here we present a model for Sea-level

1.1 What this paper is about

This paper presents SURFER, a tool for estimating the Sea level Uprise Response under Forcings of Emissions and solar Radiation management(SURFER). , that has been designed to meet all the above requirements. SURFER is a light carbon-climate-ice sheets model that captures correctly timescales from decades to millennia providing melt rates for Greenland and Antarctic ice sheets in response to emissions of CO_2 that are compatible with state of simple carbon-climate-sea level rise model based on a novel combination of conservation laws for the masses of atmospheric and oceanic carbon and for the art ice sheet models.

Our objective is to provide a tool for assessing the long-term impacts of CO_2 emissions on oceanic temperature anomalies, and of ad-hoc parametrisations for the different sea level rise and ocean acidification. We show that SURFER's outputs are compatible with the latests emission driven experiments by contributors.

It consists of 9 loosely coupled ordinary differential equations (ODEs) that are easy to understand and modify. Model simulations over 10k years (obtained with standard numerical approximations for stiff ODEs) typically run in less than 0.005 seconds on a standard laptop, see Sec. 2.5.

The model is easy to calibrate and reproduces the results of high-dimensional Earth system Models of Intermediate Complexity (EMICs) and Earth System Models (ESMs), capturing well the responses of global mean surface temperature anomaly, atmospheric carbon concentration, sea level rise and also several metrics used to assess ocean acidification ocean acidification to anthropogenic forcing.

The main focus of this paper is twofold: on the one hand, we discuss and motivate the model equations and parameters and contrast these equations and parameters to those found in similar reduced models and climate emulators. This is done in detail in Secs. 2 and 4. The aim of Sec. 2 is to establish full model transparency and, hopefully, understandability. Developing a tool for estimating the impacts of CO_2 emissions and solar radiation management measures on sea level rise and on the acidification of the oceans over millennia necessarily means making a number of choices and compromises. These choices and compromises are motivated by the intended applications and in Sec. 4 we provide recommendations for extending the model of Sec. 2 to applications that go beyond those targeted by SURFER.

On the other hand, we provide numerical evidence that, for the intended applications, SURFER can indeed reproduce the results of more sophisticated, high-dimensional earth system models. This is done in Sec. 3.

1.2 What the paper is not about

Before turning to the specification of the model equations of SURFER, let us shortly discuss what this paper is not about.

We have argued that one intended application of SURFER is that of assessing the value of CO_2 emission policies for the next decades based on sea level rise and ocean acidification under different kinds of uncertainty. We do not provide an example of such an application here. Besides the specification of an emission policy, this would also require specifying

- the uncertainties that affect the specific problem at stake,
- a function for measuring the value of possible trajectories (sometimes called a metric) and, most importantly,
- a measure for aggregating probability distributions (often the expected value measure)

for the specific problem at stake. This would go well beyond the scope of this paper but we refer the reader to (Botta et al., 2018, 2021; Helw for a discussion of the steps involved in setting up a stylised problem. Similarly, we do not apply SURFER to the computation of optimal policies (Botta et al., 2018; Helwegen et al., 2019; Carlino et al., 2020) or to the study of commitment and responsibility (Martínez Montero et al., 2022; Botta et al., 2021) under uncertainty here. Instead, we will do so in a dedicated companion paper.

A final caveat is at place: SURFER is not meant to be a “better” model than the reference ESMs it is intended to emulate in terms of climate metrics, and has not been calibrated to minimize a well-defined distance from a set of “trusted” models (see Sec. 3). Rather, SURFER is a tool that trades model complexity for speed and understandability. Both properties are crucial for the intended applications: speed is needed to tackle the computational complexity associated with uncertainty; And, under uncertainty, nothing is worse than applying a tool that one does not fully understand.

2 Model specification

SURFER consists of a system of 8 9 ordinary differential equations for the masses of carbon in four different reservoirs (atmosphere, upper ocean layer, deeper ocean layer and land), the temperature anomalies of two different reservoirs (upper ocean layer and deeper ocean layer), and the volume of Greenland and Antarctic ice sheets and sea level rise related to glaciers. Sea level rise due to the ocean thermal expansion is also taken into account through a parametrisation in terms of the ocean temperature anomalies.

Two external forcings drive the system: anthropogenic CO_2 emissions and Solar Radiation Management in the form of SO_2 aerosol injections.

The CO_2 emission rate, through the accumulation of CO_2 in the atmosphere and due to the greenhouse effect, leads to long-lasting temperature increases, while the aerosol injections, through reflecting some of the incoming solar radiation, are responsible for fast but short-lasting temperature decreases. We refer the readers to (Moreno-Cruz and Keith, 2013; Helwegen et al., 2019) (Moreno-Cruz and Keith, 2013; Helwegen et al., 2019; Robock, 2020) for more information on this form of geoengineering and to (Visioni et al., 2021) for the the latests results from the Geoengineering Model Inter-comparison Project. The CO_2 emissions are the source in the carbon cycle sub-model, which evolves the amount of carbon in the considered carbon reservoirs. The carbon concentration in the atmosphere and the aerosol injections are the driving forces of the climate sub-model, which evolves the temperature anomalies in two thermal reservoirs. Finally, the temperature anomaly of the upper ocean layer

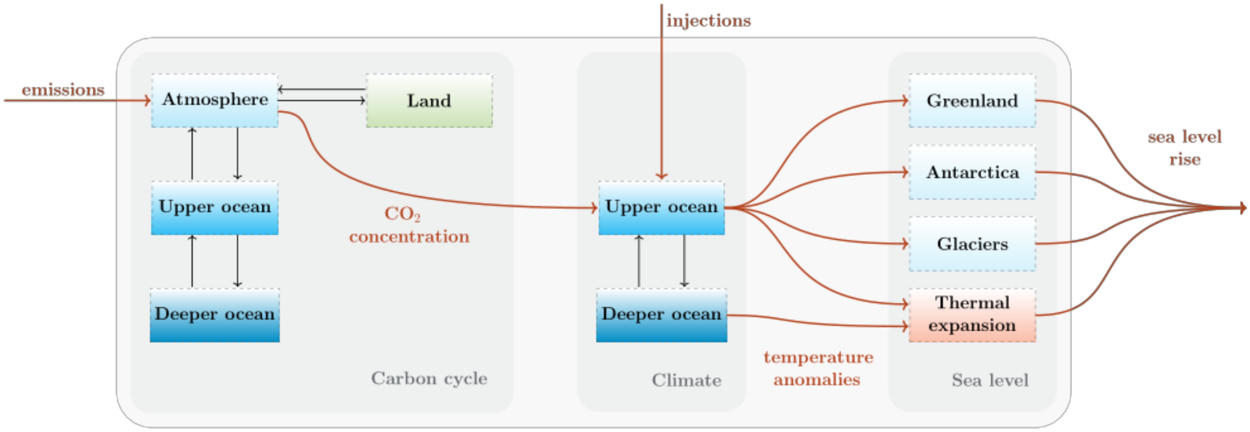

Figure 1. Conceptual diagram of SURFER. The state variables are indicated by the boxes, interactions and sources are depicted by black and dark orange arrows respectively.

(assumed in equilibrium with the atmosphere and land) forces the melting of the ice sheets ~~causing sea-level to rise. A~~ and glaciers, causing sea level to rise, while both ocean layers contribute to sea level rise due to the ocean's thermal expansion. Fig. 1 provides a conceptual diagram for the model~~can be found in Fig. 1~~. We have not included other interactions between the sub-models but we address the most relevant feedbacks in ~~the discussion section~~Sec. 4.

2.1 Carbon cycle model

The carbon cycle model is based on BEAM, a simple carbon cycle model developed by ~~Glotter et al. (2014)~~ Glotter et al. (2014) for economic and policy analyses. BEAM stands for "Bolin and Eriksson Adjusted Model" in acknowledgement of ~~Bolin and Eriksson (195~~ (Bolin and Eriksson, 1959). Since we modified the model by ~~Glotter et al. (2014)~~ Glotter et al. (2014) by including an extra carbon reservoir, a land reservoir[1], along with minor modifications to the original equations, we proceed with a full presentation of the carbon cycle model.

[1]In ~~Bolin and Eriksson (1959)~~ (Bolin and Eriksson, 1959) they include hummus and vegetation reservoirs. We have followed a different approach for obtaining the equations and fluxes corresponding to the land reservoir.

The equations for the Atmosphere (A), upper ocean layer (U), deeper ocean layer (D) and land (L) carbon reservoirs read as follows

$$\frac{dM_A}{dt} = E - F_{A\to U} - F_{A\to L}, \tag{1}$$

$$\frac{dM_U}{dt} = F_{A\to U} - F_{U\to D}, \tag{2}$$

$$\frac{dM_D}{dt} = F_{U\to D}, \tag{3}$$

$$\frac{dM_L}{dt} = F_{A\to L}, \tag{4}$$

where M_i is the mass of carbon in reservoir i, $F_{i\to j}$ the net carbon flux from reservoir i to reservoir j and E is the anthropogenic carbon emission rate. As part of the land reservoir we consider only soils and vegetation, ignoring carbon in permafrost and fossil fuel reserves. Sinks and sources associated with carbon outgassing, weathering and sediment burial are ignored because they are of secondary importance at the timescales considered here (10 yr to 5000 yr).

2.1.1 $F_{A\to U}$

Modelling the carbon flux between the atmosphere and the ocean relies on fundamental ~~aspects of~~ ocean carbonate chemistry which we now summarise (see ~~chapter~~ Ch. 8 of textbook by Sarmiento and Gruber (2006) for a deeper treatment).

When CO_2 in the atmosphere goes into the ocean it undergoes a series of chemical reactions

$$CO_{2(gas)} + H_2O \rightleftharpoons H_2CO_3^*, \tag{R1}$$

$$H_2CO_3^* \rightleftharpoons HCO_3^- + H^+, \tag{R2}$$

$$HCO_3^- \rightleftharpoons CO_3^{2-} + 2H^+, \tag{R3}$$

where $H_2CO_3^*$ represents a mix of aqueous carbon dioxide, $CO_{2(aqueous)}$, and carbonic acid, H_2CO_3[2]. The distribution between the three carbon species, $H_2CO_3^*$, HCO_3^- (bicarbonate), and CO_3^{2-} (carbonate), ~~happens~~ is fast with respect to the ocean's circulation timescale, and hence equilibrium is assumed. The equilibrium distribution relations

$$K_1 = \frac{[H^+][HCO_3^-]}{[H_2CO_3^*]}, \qquad K_2 = \frac{[H^+][CO_3^2-]}{[HCO_3^-]} \tag{5}$$

are dictated by the ocean's acidity, quantified by the proton concentration $[H^+]$. K_1 and K_2 are dissociation constants and $[H^+]$, measured in moles per kilogram, relates to the ocean pH as

$$pH = -\log_{10}[H^+]. \tag{6}$$

[2] It is common practice to consider these two species of carbon together into a single variable because they are difficult to distinguish from each other (Sarmiento and Gruber, 2006, Ch. 8.2).

The total dissolved inorganic carbon (DIC) can then be written as

$$\begin{aligned} \mathrm{DIC} &= [\mathrm{H_2CO_3^*}] + [\mathrm{HCO_3^-}] + [\mathrm{CO_3^{2-}}] \\ &= \left(1 + \frac{K_1}{[\mathrm{H^+}]} + \frac{K_1 K_2}{[\mathrm{H^+}]^2}\right)[\mathrm{H_2CO_3^*}]. \end{aligned} \tag{7}$$

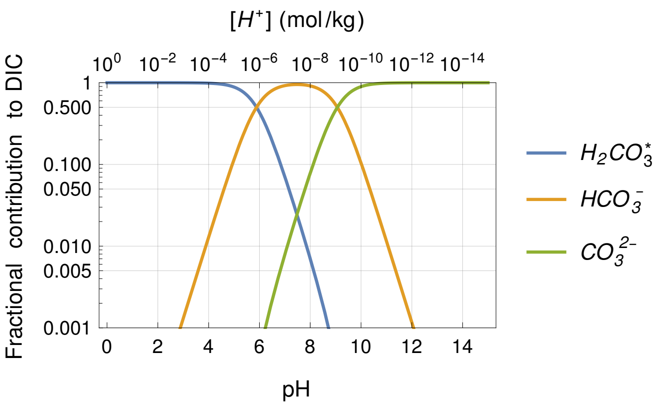

Figure 2. Carbon species fractional contribution to DIC for varying pH.

In Fig. 2 we show the fractional ~~contribution~~ contributions of the different carbon species to DIC for varying pH. For the present pH value of around 8 we can see in Fig. 2 that bicarbonate is the dominant carbon ~~specie~~ species in the ocean. From the chemical reactions (R1), (R2) and (R3) we see that when CO_2 dissolves in the ocean, hydrogen ions are released and ocean acidifies. This in turn means that the proportion of carbonate decreases and that of $H_2CO_3^*$ increases. The alkalinity however, defined as the excess of bases over acids

$$Q = [\mathrm{HCO_3^-}] + 2[\mathrm{CO_3^{2-}}] + [\mathrm{OH^-}] - [\mathrm{H^+}] + [\mathrm{B(OH)_4^-}] + \text{minor bases}\,, \tag{8}$$

does not change with those reactions. Since no other reactions are accounted for in this carbon cycle model the alkalinity ~~remains~~ is constant. This assumption will lead to stronger than expected acidification on long timescales (~ 4000 years) in which calcium carbonate production, dissolution and burial (not accounted for here) are significant. As it is usual practice, we will approximate the alkalinity[3] by its dominant terms, that is by the carbonate alkalinity

$$Q \approx [\mathrm{HCO_3^-}] + 2[\mathrm{CO_3^{2-}}] = \left(\frac{K_1}{[\mathrm{H^+}]} + \frac{2K_1K_2}{[\mathrm{H^+}]^2}\right)[\mathrm{H_2CO_3^*}]. \tag{9}$$

The flow of CO_2 between the atmosphere and upper ocean layer is proportional to the difference in CO_2 partial pressures

$$F_{A\to U} \propto \left(p^A_{\mathrm{CO_2}} - p^U_{\mathrm{CO_2}}\right) \tag{10}$$

and by writing the partial pressures as proportional to the corresponding carbon masses

$$F_{A\to U} = -k_{A\to U}M_A + k_{U\to A}M'_U \tag{11}$$

[3] See e.g., ~~Chapter~~ Ch. 8 ~~section~~ Sec. 8.2 of ~~Sarmiento and Gruber (2006)~~ Sarmiento and Gruber (2006) for more details on this.

where $p^U_{CO_2}$ refers to the partial pressure of carbon in the form $H_2CO_3^*$, and M'_U to the corresponding carbon mass. The parameters $k_{i\to j}$ are the transport coefficients from reservoir i to reservoir j.

The equilibrium concentration of $H_2CO_3^*$ in the ocean, corresponding to an atmospheric CO_2 partial pressure $p^A_{CO_2}$ can be determined through the CO_2 solubility constant

$$K_0 = \frac{[H_2CO_3^*]}{p_{CO_2}}, \tag{12}$$

where ~~have written~~ p_{CO_2} is written without a reservoir index because~~in equilibrium~~, when in equilibrium, atmospheric and upper ocean have the same CO_2 partial pressure.

2.1.2 $F_{U\to D}$

The exchange of carbon between the two ocean layers is ruled by oceanic currents and therefore depends on the total dissolved inorganic carbon in each layer

$$F_{U\to D} = k_{U\to D} M_U - k_{D\to U} M_D. \tag{13}$$

This is in contrast with the carbon exchange between the upper ocean to atmosphere which depends on the upper ocean carbon concentration in the form of $H_2CO_3^*$. Now we can write the carbon cycle equations as

$$\frac{dM_A}{dt} = E - k_{A\to U} M_A + k_{U\to A} M'_U - F_{A\to L}, \tag{14a}$$

$$\frac{dM_U}{dt} = k_{A\to U} M_A - k_{U\to A} M'_U - k_{U\to D} M_U + k_{D\to U} M_D, \tag{14b}$$

$$\frac{dM_D}{dt} = k_{U\to D} M_U - k_{D\to U} M_D, \tag{14c}$$

$$\frac{dM_L}{dt} = F_{A\to L}. \tag{14d}$$

Following Bolin and Eriksson (1959) we assume that the four reservoirs were in equilibrium ~~in~~ at pre-industrial times (with $E(t_{PI}) = 0$) and we examine the equilibrium equations

$$0 = -k_{A\to U} M_A(t_{PI}) + k_{U\to A} M'_U(t_{PI}) - F_{A\to L}(t_{PI}), \tag{15a}$$

$$0 = k_{A\to U} M_A(t_{PI}) - k_{U\to A} M'_U(t_{PI}) - k_{U\to D} M_U(t_{PI}) + k_{D\to U} M_D(t_{PI}), \tag{15b}$$

$$0 = k_{U\to D} M_U(t_{PI}) - k_{D\to U} M_D(t_{PI}), \tag{15c}$$

$$0 = F_{A\to L}(t_{PI}). \tag{15d}$$

These allow to relate transport coefficients

$$k_{A\to U} = k_{U\to A} \frac{M'_U(t_{PI})}{M_A(t_{PI})}, \tag{16}$$

$$k_{U\to D} = k_{D\to U} \frac{M_D(t_{PI})}{M_U(t_{PI})}, \tag{17}$$

where we can further write

$$M'_U = [\mathrm{H_2CO_3^*}]\, W_U\, \bar{m}_C$$

$$M_A = \text{moles of } \mathrm{CO_2} \text{ in atmosphere} \times \bar{m}_C,$$

$$M_{(U,D)} = \mathrm{DIC}_{(U,D)}\, W_{(U,D)}\, \bar{m}_C,$$

where W_U and W_D stand for the whole mass of the upper and deeper ocean layers and can be approximated by

$$W_U \approx m_O\, \bar{m}_W\, \frac{h_U}{h_U + h_D}, \quad W_D \approx m_O\, \bar{m}_W\, \frac{h_D}{h_U + h_D}, \tag{18}$$

with m_O the moles of water in the ocean, $\bar{m}_W$ the molar mass of H_2O, $\bar{m}_C$ the molar mass of carbon and h_U and h_D the thicknesses of the ocean layers. Considering the equilibrium solubility relation (12) and

$$p^A_{\mathrm{CO_2}} = 1(\text{atm}) \frac{\text{moles of } \mathrm{CO_2} \text{ in atmosphere}}{\text{moles in atmosphere}}$$

we arrive at

$$k_{A\to U} = k_{U\to A} \frac{M'_U(t_{PI})}{M_A(t_{PI})} = k_{U\to A} \frac{W_U\, K_0}{m_A}, \tag{19}$$

$$k_{U\to D} = k_{D\to U} \frac{M_D(t_{PI})}{M_U(t_{PI})} = k_{D\to U}\, \delta_{\mathrm{DIC}}\, \frac{h_D}{h_U}, \tag{20}$$

where m_A are the moles of air in the atmosphere and

$$\delta_{\mathrm{DIC}} = \frac{\mathrm{DIC}_D(t_{PI})}{\mathrm{DIC}_U(t_{PI})} \tag{21}$$

where $\mathrm{DIC}_U(t_{PI})$ and $\mathrm{DIC}_D(t_{PI})$ are the pre-industrial DIC concentration in upper and lower ocean layers. ~~This parameter is a way to take into account the biological and carbonate pumps as it~~ The parameter δ_{DIC} specifies the DIC gradient between the two ocean layers and effectively accounts for the biological and carbonate pumps.

The next step is to express the carbon mass in $H_2CO_3^*$ form, M'_U, in Eqs. (14) as a function of the state variables. We begin by

$$\frac{M'_U}{M_U} = \frac{[\mathrm{H_2CO_3^*}]_U}{\mathrm{DIC}_U} = \left(1 + \frac{K_1}{[\mathrm{H^+}]_U} + \frac{K_1 K_2}{[\mathrm{H^+}]^2{}_U}\right)^{-1}.$$

Using the definitions of DIC and carbonate alkalinity (Q in Eq. (9)), and the relation of DIC_i with carbon mass M_i, $[\mathrm{H^+}]_i$ can be solved for in terms of M_i

$$[\mathrm{H^+}]_i = \frac{K_1}{2\tilde{Q}_i} \left(\sqrt{(M_i - \tilde{Q}_i)^2 - 4\frac{K_2}{K_1}\tilde{Q}_i(\tilde{Q}_i - 2M_i)} + (M_i - \tilde{Q}_i) \right) \tag{22}$$

with $i = U$ or D and where

$$\tilde{Q}_i = Q_i\, W_i\, \bar{m}_C$$

is the carbon mass corresponding to the carbonate alkalinity. The factor tracking the ocean's buffer capacity becomes

$$B(M_U) \equiv \frac{M'_U}{M_U} = \frac{1}{2} - \frac{\tilde{Q}_U}{2M_U} + \frac{K_1 \sqrt{(M_U - \tilde{Q}_U)^2 - 4\frac{K_2}{K_1}\tilde{Q}_U(\tilde{Q}_U - 2M_U)} - 4M_U K_2}{2M_U(K_1 - 4K_2)}. \tag{23}$$

2.1.3 $F_{A\rightarrow L}$

Now we turn to the equation for the land reservoir. The proposed equation is not process based, it is instead based on the output of the Zero Emissions Commitment Model Inter-comparison Project (ZECMIP) (Jones et al., 2019; MacDougall et al., 2020) experiments by different EMICs and ESMs.

We analysed the output of the ZECMIP experiments B1 and B3 in (Jones et al., 2019; MacDougall et al., 2020), and observed that the land carbon anomaly relaxes to a value proportional to the atmospheric carbon anomaly after typically 4 to 6 decades. This behaviour can be captured by the following relation:

$$\delta M_L(t) = \alpha_L \delta M_A(t), \tag{24}$$

where $\delta M_i(t) = M_i(t) - M_i(t_{PI})$. The values of α_L approached by the different models in B1 experiments (lower cumulated emissions) tend to be higher than the ones approached by the higher cumulated emissions experiment B3. We noticed that the quantity

$$\frac{\delta M_L(t)}{\delta M_A(t)} \frac{M_A(t)}{M_A(t_{PI})} \tag{25}$$

tends to approach a ~~model dependent~~ model-dependent constant value, say β_L, which is independent of the cumulated emissions after ~~4 to 6~~ four to six decades. Based on these observations we propose the following equation for the land carbon anomaly δM_L

$$\frac{d\delta M_L}{dt} = k_{A\rightarrow L}\left(\beta_L \frac{M_A(t_{PI})}{M_A}\delta M_A - \delta M_L\right). \tag{26}$$

With this equation δM_L relaxes to an equilibrium value proportional to the ratio $\frac{\delta M_A}{M_A}$. This dependency can be interpreted as the result of two competing processes : CO2 fertilization ($\propto \delta M_A$) and an enhanced bacterial respiration due to climate change ($\propto M_A$)

The final equations for the carbon cycle can now be written as

$$\frac{dM_A}{dt} = E(t) - k_{A\rightarrow U}\left(M_A - \frac{m_A}{W_U K_0} B(M_U) M_U\right) - k_{A\rightarrow L}\left(\beta_L M_A(t_{PI})\left(1 - \frac{M_A(t_{PI})}{M_A}\right) - (M_L - M_L(t_{PI}))\right), \tag{27a}$$

$$\frac{dM_U}{dt} = k_{A\rightarrow U}\left(M_A - \frac{m_A}{W_U K_0} B(M_U) M_U\right) - k_{U\rightarrow D}\left(M_U - \frac{1}{\delta_{\text{DIC}}}\frac{h_U}{h_D} M_D\right), \tag{27b}$$

$$\frac{dM_D}{dt} = k_{U\rightarrow D}\left(M_U - \frac{1}{\delta_{\text{DIC}}}\frac{h_U}{h_D} M_D\right), \tag{27c}$$

$$\frac{dM_L}{dt} = k_{A\rightarrow L}\left(\beta_L M_A(t_{PI})\left(1 - \frac{M_A(t_{PI})}{M_A}\right) - (M_L - M_L(t_{PI}))\right). \tag{27d}$$

Equations (27) are very similar to the ones presented by ~~Glotter et al. (2014)~~ Glotter et al. (2014) but with the following important differences:

1. There is a land carbon reservoir~~, this is an important~~. This update to the ~~Glotter et al. (2014) model as it~~ Glotter et al. (2014) model improves the agreement with most recent results from EMICs and ESMs.

2. The ocean buffer factor is explicitly written in terms of M_U to highlight the non-linear nature of the model.

3. The relation between the transport coefficients between the two ocean layers here depends not only on the ratio of the thickness of the layers (δ) but also on the ratio of their pre-industrial concentration of dissolved inorganic carbon (δ_{DIC}). This allows for an equilibrium solution in which the dissolved inorganic carbon concentration is different in the upper and lower layerlayers, which is known to be the case due to the soft tissue and carbonate pumps. Even if SURFER does not explicitly consider those two pumps, including the pre-industrial DIC ratio of the two ocean layers yields better results for ocean acidification related quantities than assuming same carbon concentration at equilibrium.

The presented carbon cycle equations for atmosphere and ocean (and also the ones in Ref. Glotter et al. (2014)) look very (Glotter et al., 2014)) are similar to the ones considered in DICE, the Dynamic Integrated model of Climate and the Economy (Nordhaus, 1992, 2013). The big difference between the two is that the upper ocean buffer factor B is considered to be constant in DICE while in SURFER it evolves with the ocean acidification. By including the non-linearities due to ocean carbonate chemistry, SURFER's carbon cycle, as the one by Glotter et al. (2014)Glotter et al. (2014), captures the fact that as the ocean takes in CO_2 from the atmosphere it becomes a worse sink for future CO_2 intake. This enables the correct tracking of carbon concentrations up to timescales of several thousands of years, which is impossible with a linear model like DICE. One of the main objectives of the present contribution is to provide a model of sea level rise caused by ice sheet melting which is a slow process lasting several thousands of years. As explained by Archer et al. (2009), a linear carbon cycle is inadequate for such long-term purposes.

Another benefit of SURFER's carbon cycle is the tracking of the pH and the concentrations of the different carbon species in the ocean; this can be done a posteriori, using the obtained $M_U(t)$ together with Eqs. (22), (6), (9) and (5). SURFER can thus be of use for policy analyses that deal with ocean acidification.

Ocean acidification destabilises marine ecosystems making it more difficult for shellfish and corals to grow. As such, ocean acidification is one of the 9 identified planetary boundaries (Rockström et al., 2009; Steffen et al., 2015). This planetary boundary has however not been quantified in terms of pH, it. It is instead given in terms of the aragonite saturation state which can be approximated as

$$\Omega_{\mathrm{ar}} \approx \frac{[\mathrm{CO}_3^{2-}]}{[\mathrm{CO}_3^{2-}]_{\text{saturation ar}}}, \tag{28}$$

where $[\mathrm{CO}_3^{2-}]$ is the carbonate concentration in the ocean and $[\mathrm{CO}_3^{2-}]_{\text{saturation ar}}$ is the carbonate concentration at which aragonite is saturated[4]. Aragonite is the most vulnerable form of calcium carbonate and its saturation state relates in a more straightforward way to some forms of marine life than pH. A value of $\Omega_{\mathrm{ar}} < 1$ means that aragonite dissolves but organisms struggle to grow and thrive already at bigger values of Ω_{ar}. The planetary boundary is set at 80% of the pre-industrial value which was $\Omega_{\mathrm{ar}}(t_{PI}) = 3.44$.

[4] $[\mathrm{CO}_3^{2-}]_{\text{saturation ar}}$ depends strongly on pressure and hence changes along the water column.

2.2 Climate model with solar radiation management

SURFER's climate sub-model is a linear 2-box model, similar to those in (Gregory, 2000; Held et al., 2010), for the evolution of the upper and deeper ocean temperature anomalies , δT_U and δT_Drespectively , respectively (measured in °C)

$$c_{vol}\, h_U \frac{d\delta T_U}{dt} = \beta \left(\frac{F(M_A, I)}{\beta} - \delta T_U \right) - \gamma \left(\delta T_U - \delta T_D \right), \tag{29}$$

$$c_{vol}\, h_D \frac{d\delta T_D}{dt} = \gamma \left(\delta T_U - \delta T_D \right). \tag{30}$$

The atmosphere is assumed to be in thermal equilibrium with the upper ocean layer. Due to this, and the fact that the upper ocean heat capacity is much bigger than that of the atmosphere, the atmosphere is not explicitly part of the climate sub-model and the radiative forcings are applied to the upper ocean layer. The constant c_{vol} is the seawater's volumetric heat capacity, obtained by multiplying the specific heat capacity of seawater and the density of seawater. The thicknesses h_U and h_D of the two ocean layers are the same as for the carbon cycle. The γ is thermal conductivity between the ocean layers is denoted by γ and β is the climate feedback parameter related to the equilibrium climate sensitivity (in °C)

$$\mathrm{ECS} = \frac{F_{2X}}{\beta}, \tag{31}$$

with F_{2X} the radiative forcing corresponding to a doubling of CO_2. The anthropogenic radiative forcing (measured in W m^{-2}) in Eq. (29) responsible for the temperature anomalies consists of two terms,

$$F(M_A, I) = F_{2X} \log_2 \left(\frac{M_A}{M_A(t_{PI})} \right) - \alpha_{SO2 SO_2} \exp \left(-(\beta_{SO2 SO_2}/I)^{\gamma_{SO2}\gamma_{SO_2}} \right), \tag{32}$$

a first one corresponding to the standard greenhouse effect and a second one corresponding to solar radiation management in the form of aerosol injection. The solar radiation management term comes from (Niemeier and Timmreck, 2015). The variable I corresponds to the sulfur injection rate and is in general time dependent. α_{SO_2}, β_{SO_2} and γ_{SO_2} are the fitting parameters considered in (Niemeier and Timmreck, 2015).

2.3 Sea level rise

Four different components contribute to SURFER's estimation of sea level rise: ocean thermal expansion, glaciers and two ice sheets

$$S_{tot} = S_{th} + S_{gl} + S_{GIS} + S_{AIS}, \tag{33}$$

where S_{tot} is the total sea level rise and S_{th}, S_{gl}, S_{GIS} and S_{AIS} are the ocean thermal expansion, glacier, Greenland ice sheet and Antarctic ice sheet contributions, respectively. While ocean thermal expansion and glaciers are the first contributors to sea level rise on the short timescales of decades, on the longer timescales of centuries and millennia, the biggest contributions come from the ice sheets.

2.3.1 Ocean thermal expansion

The ocean thermal expansion parametrisation relies on the ocean data (layers sizes and temperature anomalies) that is part of SURFER's climate sub-model. This contribution to sea level rise is then computed as

$$S_{th} = \alpha_U h_U \delta T_U + \alpha_D h_D \delta T_D \quad (34)$$

where α_i is the thermal expansion coefficient corresponding to the i layer (in °C^{-1}), h_i is the size of the i layer (in meters) and δT_i is the temperature anomaly (in °C) with respect to to pre-industrial times of the i layer. We consider that the expansion coefficients of the two layers have different values to capture the fact that surface waters have bigger thermal expansion coefficients than deeper denser waters as shown, for example, in Fig. 1(c) of (Williams et al., 2012). As a simplification, we neglect the size change of the ocean layers $h_{(U,D)}$ due to sea level rise and we also assume that the expansion coefficients are constant in time.

The sea level rise contribution from ocean thermal expansion comes from both ocean layers. In the timescales of decades and a couple of centuries, the deeper ocean layer does not contribute much due to its thermal inertia. As the deeper ocean warms up, in the timescale of thousands of years, it can become the main contributor to S_{th}. Figure 3a shows the sea level rise commitment from ocean expansion once thermal equilibrium has been achieved between the two ocean layers, that is, with $\delta T_U = \delta T_D$.

2.3.2 Glaciers

The sea level rise contribution from glaciers is modelled with an ordinary differential equation that relaxes the current sea level rise value due to glaciers, S_{gl}, to its expected equilibrium value for the current temperature $S_{gl\,eq}(\delta T_U)$

$$\frac{dS_{gl}}{dt} = \frac{1}{\tau_{gl}} \left(S_{gl\,eq}(\delta T_U) - S_{gl} \right), \quad (35)$$

where τ_{gl} is the relaxation timescale. The same form of equation was used by Mengel et al. (2016), although with a differently parametrised $S_{gl\,eq}$. Levermann et al. (2013) analysed the sea level commitments of different sea level rise components depending on the forcing temperature. They estimate the shape of such $S_{gl\,eq}(\delta T_U)$ for all land glaciers excluding ice sheets (see Fig. 1B in (Levermann et al., 2013)) which we will approximate as

$$S_{gl\,eq}(\delta T_U) = S_{gl\,pot} \tanh\left(\frac{\delta T_U}{\zeta} \right), \quad (36)$$

where $S_{gl\,pot}$ is the potential sea level rise due to glaciers, which corresponds to all the ice volume in glaciers in units of sea level rise equivalent, and ζ is a sensitivity coefficient. Figure 3b shows the shape of $S_{gl\,eq}$ for the suggested values of $S_{gl\,pot}$ and ζ in Table 6.

2.4 ~~Ice sheets and sea level rise~~

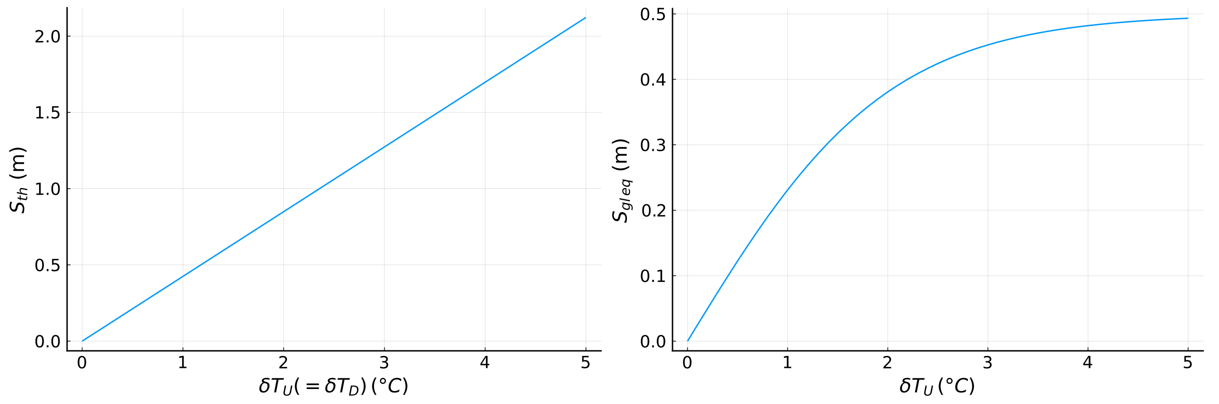

(a) Ocean thermal expansion commitment

(b) Glacier sea level rise commitment

Figure 3. Equilibrium sea level rise contribution from ocean thermal expansion and glaciers.

This way of modelling the glaciers has a couple of advantages to similar methods used in other simple models. First of all, the formulation is fully transparent and nothing more than equations (35) and (36) are needed. As for the behavior, it captures some expected physics:

1. No forcing corresponds to no sea level rise from glaciers.
2. For small enough forcings, different levels of forcing lead to different levels of sea level rise.
3. Different levels of forcing on the same initial state generate different rates of sea level rise.
4. There is a cap on the maximum amount of sea level rise that can come from glaciers.

2.3.1 Ice sheets

Multi-stability regions and tipping points have been identified both for the Greenland and Antarctic ice sheets (e.g., Lenton et al., 2008; Letreguilly et al., 1991; Pattyn, 2006; Ridley et al., 2010; Robinson et al., 2012; Gregory et al., 2020; Garbe et al., 2020). The proposed ice sheet model highlights those tipping points and is easy to adapt to ~~capture the dynamics of these two ice sheets~~ both ice sheets such that it captures their dynamics. The state variable is the volume fraction of ice with respect to a reference state, which we set to be the ice sheet's pre-industrial state. The ice sheets' contributions sea level rise with respect to pre-industrial times is computed as a function of the ice sheets' melted fractions of ice and their total sea level rise potential

$$S_{GIS} = S_{GIS\,pot}(1 - V_{GIS}(t)), \quad S_{AIS} = S_{AIS\,pot}(1 - V_{AIS}(t)), \tag{37}$$

where $S_{GIS\,pot}$ and $S_{AIS\,pot}$ are the sea level rise potentials of Greenland's and Antarctic ice sheet respectively, and V_{GIS} and V_{AIS} their volume fraction with respect to their pre-industrial volume.

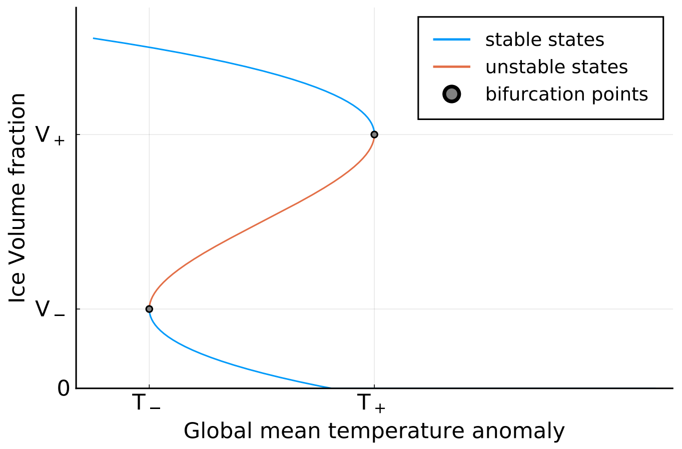

Figure 4. Ice sheet steady states for model defined in eqs. (38) and (39).

To capture the dynamics of an ice sheet featuring multi-stability and tipping points we propose a non linear ordinary differential equation for the ice volume fraction

$$\frac{dV}{dt} = \mu(V, \delta T_U)\left(-V^3 + a_2 V^2 + a_1 V + c_1 \delta T_U + c_0\right), \tag{38}$$

where the third-order polynomial of the volume fraction and the term proportional to a forcing temperature imply a double fold bifurcation diagram for the steady states in terms of a constant forcing temperature, see Fig. 4. In contrast to the ocean part of the carbon cycle model and climate model presented before, the ice sheet model is not explicitly derived from physical processes; it is a generic dynamical system model based on the concept of a double-fold bifurcation to be calibrated on state-of-the-art ice sheet models' output. In that sense, it is an emulator. The different terms of the polynomial are not there because they represent specific physical processes but because as a whole they produce the desired steady-state structure. The constant parameters (a_2, a_1, c_1, c_0) are given in terms of the bifurcation points $((T_+, V_+), (T_-, V_-))$ as

$$a_2 = \frac{3(V_- + V_+)}{2}, \tag{39a}$$

$$a_1 = -3V_- V_+, \tag{39b}$$

$$c_1 = -\frac{(V_+ - V_-)^3}{2(T_+ - T_-)}, \tag{39c}$$

$$c_0 = +\frac{T_+ V_-^2 (V_- - 3V_+) - T_- V_+^2 (V_+ - 3V_-)}{2(T_- - T_+)}, \tag{39d}$$

which are the quantities which determine the steady-state structure of the system, see Fig. 4. Since we want to impose the additional constraint of there existing a steady-state ice volume fraction of 1 at temperature anomaly equal to 0, the number of free parameters is reduced by one by setting

$$V_- = \frac{-2 + V_+\left(1 + G^{1/3} + G^{-1/3}\right)}{-1 + G^{1/3} + G^{-1/3}} \tag{40}$$

with

$$G = \left(\frac{T_+ + T_- + 2\sqrt{T_- T_+}}{T_+ - T_-} \right). \tag{41}$$

Instead of fixing the 4 parameters $((T_+, V_+), (T_-, V_-))$ independently, V_- is given in terms of the other three such that the pre-industrial reference state condition $V_{eq}(\delta T_U = 0) = 1$ is satisfied.

The evolution is further affected by the forcing temperature δT_U and inverse timescale

$$\mu(V, \delta T_U) = \begin{cases} 1/\tau_+ & \text{if } H > 0, \\ 1/\tau_- & \text{if } H < 0 \text{ and } V > 0, \\ 0 & \text{if } H < 0 \text{ and } V = 0, \end{cases} \tag{42}$$

with

$$H = \left(-V^3 + a_2 V^2 + a_1 V + c_1 \delta T_U + c_0 \right). \tag{43}$$

We write $\mu(V, \delta T_U)$ as a function of the state variables V and δT_U in such a way that it can take 3 different constant values. This is done to reflect the ~~fact that there is a~~ timescale asymmetry between the processes of melting and freezing ice and to ensure that the ice fraction remains bigger ~~ot~~ or equal to zero.

2.4 ~~Units, parameters~~ Calibration and initial conditions

In this section we give the values and units of the parameters used to run the model. We also provide an explanation of how we have fixed some of them and obtained the pre-industrial initial conditions that we use in Sec. 3.

Parameters and initial conditions for the carbon cycle model can be found in Tables 1 and 2, the parameters for the climate model are in Table 3 and the ones for ~~the ice sheet model~~ sea level rise can be found in Tables 4, 5 and 6 for the ocean thermal expansion, glaciers and ice sheet (adapted to Greenland and Antarctica) ~~can be found in Table 6~~models respectively. All examples in this paper ~~will~~ start from pre-industrial conditions, which for the climate and ~~ice sheet~~ sea level rise models are trivial, ~~$\delta T_{(U,D)}(t_{PI}) = 0$, $V_{(G,A)}(t_{PI}) = 1$~~$\delta T_U(t_{PI}) = \delta T_D(t_{PI}) = 0$, $S_{gl}(t_{PI}) = 0$, $V_{GIS}(t_{PI}) = V_{AIS}(t_{PI}) = 1$.

2.4.1 Carbon cycle

The dissociation parameters K_1 and K_2, the CO_2 solubility K_0, and the alkalinity Q are assumed to be constant. A temperature (T) and salinity (S) dependent alternative is provided for K_1, K_2 and K_0 in (Sarmiento and Gruber, 2006, Pg. 325)[5]. The specific values that we will be using for the constants K_1, K_2 and K_0 have been obtained from the expressions in (Sarmiento and Gruber, 2006). We fix the parameter δ_{DIC} to 1.15 in accordance with data provided in (Sarmiento and Gruber, 2006, Pg. 320).

[5] Similar expressions are given in ~~Ref. Glotter et al. (2014)~~(Glotter et al., 2014)

We fix the parameters K_1, K_2 and K_0 in the carbon cycle model by ensuring that initial conditions are consistent with pre-industrial data. The parameter $\delta = h_D/h_U$, also playing a role in the initial conditions, has been set to $\delta = 20$, which is a middle ground between the thermal box sizes of (Gregory, 2000; Held et al., 2010) and the ratio of sizes suggested in (Bolin and Eriksson, 1959; Glotter et al., 2014), the reason for the chosen value is provided below. Other parameters, like $k_{A\to U}$, $k_{U\to D}$ and $k_{A\to L}$ have been adjusted to match the dynamics of more complex carbon cycle models. We now proceed with a more in depth explanation.

In pre-industrial times the atmospheric CO_2 concentration was 280ppm which corresponds to an atmospheric carbon mass

$$\begin{aligned} M_A(t_{PI}) &= \text{moles of CO}_2 \text{ in atmosphere}(t_{PI}) \times \bar{m}_C \\ &= 280 \times 10^{-6}\, m_A\, \bar{m}_C = 580.3 \text{ PgC}. \end{aligned}$$

where $\bar{m}_C$ is the Carbon molar mass. We assume that in pre-industrial conditions the carbon cycle was in equilibrium. Additionally we impose that the total mass of carbon in the ocean was 38000 PgC. Using the relations between ocean carbon masses, the corresponding DICs and the equilibrium equations we can write

$$\begin{aligned} M_U(t_{PI}) + M_D(t_{PI}) &= \text{DIC}_U(t_{PI})\, m_O \bar{m}_\text{C} \bar{m}_\text{W} \frac{1+\delta_\text{DIC}\,\delta}{1+\delta} \\ &= 38000 \text{ PgC} \end{aligned} \tag{44}$$

where we have written the carbon and water molar masses as $\bar{m}_{(\text{C,W})}$. We see that $\delta = 20$ implies a reasonable value of $\text{DIC}_U(t_{PI}) = 1973.53\,\mu\text{mol kg}^{-1}$ [6]by comparing to global average data in Fig. 8.1.2 of (Sarmiento and Gruber, 2006) and to global averages from ZECMIP, see pre-industrial range of values in DIC plot in Fig. 9. This value of DIC is one of the ingredients used to fix the dissociation and solubility constants.

The pH of the upper ocean in pre-industrial times was around 8.2. Here we will fix it to 8.17 in accordance ~~to~~ with historical CMIP6 results in (Gutiérrez et al., 2021) which implies a Hydrogen ion concentration of $[\text{H}^+](t_{PI}) = 10^{-8.17}$ mol kg^{-1}. Q_U and DIC_U at pre-industrial time can be written as

$$\begin{aligned} Q_U &= \left(\frac{K_1}{[\text{H}^+](t_{PI})} + \frac{2K_1K_2}{\left([\text{H}^+](t_{PI})\right)^2} \right) K_0\, p^A_{\text{CO}_2}(t_{PI}), \\ \text{DIC}_U(t_{PI}) &= \left(1 + \frac{K_1}{[\text{H}^+](t_{PI})} + \frac{K_1K_2}{\left([\text{H}^+](t_{PI})\right)^2} \right) K_0\, p^A_{\text{CO}_2}(t_{PI}) \end{aligned}$$

where $p^A_{\text{CO}_2}(t_{PI}) = 280 \times 10^{-6}$ atm. We use these relations to fix the dissociation and solubility constants. First, we impose an alkalinity value compatible with observations $Q_U = 2200\,\mu\text{mol kg}^{-1}$. Second, we impose the already fixed value of $\text{DIC}_U(t_{PI}) = 1973.53\,\mu\text{mol kg}^{-1}$. Third, we use the temperature (T) and salinity (S) dependent expressions for the dissociation and solubility given in (Sarmiento and Gruber, 2006). Last, we solve the system of two equations for T and S numerically. Such a procedure yields "effective" $T = 294.7$K and $S = 32.49‰$ a warmer and slightly less salty ocean than the global averages, but they determine dissociation constants which, in the end, yield realistic carbon masses, concentrations, and alkalinity in the pre-industrial ocean.

[6] ~~This value of DIC is one of the ingredients used to fix the dissociation and solubility constants~~

We ignore the temperature dependence of the carbonate concentration corresponding to aragonite saturation and we fix it to

$$[\mathrm{CO}_3^{2-}]_{\text{saturation ar}} = \frac{[\mathrm{CO}_3^{2-}](t_{PI})}{\Omega_{\text{ar}}(t_{PI})} \tag{45}$$

where $[\mathrm{CO}_3^{-2}](t_{PI})$ is obtained through Eqs. (5) and (12) and $\Omega_{\text{ar}}(t_{PI}) = 3.44$ from (Rockström et al., 2009; Steffen et al., 2015).

The ZECMIP B1 and B3 experiments' outputs suggest a land carbon parameter β_L between 0.5 and 2.3 We ~~settled~~ settle for 1.7 but the choice is not critical. This value is closer to those of ESMs than to those of the EMICs as can be seen in be bottom right plot of Figs. 9 and 10. The pre-industrial mass of land carbon is set to 2200 PgC for plotting purposes but this quantity does not affect the land carbon uptake.

Finally, for the inverse timescale $k_{A\to U}$ we ~~kept he~~ take the value recommended by Glotter et al. (2014). $k_{U\to D}$ ~~was~~ is fixed to obtain a timescale for the deep ocean dynamics of 1000 years $k_{U\to D} = \delta\,\delta_{\text{DIC}}/1000$. The inverse timescale $k_{A\to L}$ ~~was~~ is fixed to match the output of ZECMIP B1 and B3 experiments.

Users of the model are invited to explore other possibilities of fixing parameters but in this paper we will restrict ourselves to using SURFER only with the supplied parameters and initial conditions and we ~~will~~ show that, despite its simplicity, its predictions are in excellent agreement with more complex models.

2.4.2 Climate

In the climate model we need to fix the parameters h_U (or h_D, since the ratio δ has already been fixed), c_{vol}, F_{2X}, β, γ, and the parameters from the aerosol forcing α_{SO_2}, β_{SO_2}, γ_{SO_2}. The values adopted in the following are listed on Table 3.

The sea water volumetric heat capacity c_{vol} is obtained by multiplying the specific heat capacity of seawater, which is taken to be 3850 J kg^{-1} °C^{-1} and the density of seawater, taken to be 1027 kg m^{-3}. The extra radiative forcing due to a doubling concentration of CO_2, F_{2X}, ~~comes from the 6th IPCC~~ has been chosen according to the IPCC 6th Assessment Report (Arias et al., 2021) and parameter h_U ~~comes from~~ according to (Gregory, 2000). β and γ have been fixed to yield Equilibrium Climate Sensitivity and Transient Climate Response

$$\mathrm{ECS} = \frac{F_{2X}}{\beta} = 3.5\ ^\circ\mathrm{C}, \quad \mathrm{TCR} = \frac{F_{2X}}{\beta+\gamma} = 2.0\ ^\circ\mathrm{C}, \tag{46}$$

compatible with results in the 6th IPCC Assessment Report (Arias et al., 2021), i.e., ECS very likely [2 to 5] °C and TCR very likely [1.4 to 2.2] °C . Aerosol forcing parameters come from the work of Niemeier and Timmreck (2015).

2.4.3 Ocean thermal expansion

The thermal expansion coefficients α_U and α_D in Eq. (34) have been first estimated by looking at the thermal expansion coefficient profile along the water column presented in Fig. 1(c) of (Williams et al., 2012) and taking into account the sizes of h_U and h_D in SURFER. Then they have been slightly corrected to better match the long-term trends presented by Van Breedam et al. (2020) . Figures 5 and 16 show the performance of SURFER's thermal expansion parametrisation against other models both on short and long timescales.

~~Quantity~~ Parameter	Value
δ	20
δ_{DIC}	1.15
K_0	3.148×10^{-2} mol (kg atm)$^{-1}$
K_1	1.326×10^{-6} mol kg^{-1}
K_2	9.198×10^{-10} mol kg^{-1}
m_A	1.727×10^{20} mol
m_O	7.8×10^{22} mol
$\bar{m}_C$	12×10^{-3} kg mol^{-1}
$\bar{m}_W$	18×10^{-3} kg mol^{-1}
Q_U	2.2×10^{-3} mol kg^{-1}
$\tilde{Q}_U$	1765.0 PgC
$[CO_3^{2-}]_{\text{saturation ar}}$	68.40 μmol kg^{-1}
$k_{A\to U}$	0.25 yr^{-1}
$k_{U\to D}$	0.023 yr^{-1}
~~$k_{U\to L}$~~ $k_{A\to L}$	0.025 yr^{-1}
β_L	1.7

Table 1. ~~Values of parameters~~ Parameter values for the carbon cycle model.

Quantity	Value
$M_A(t_{PI})$	580.3 PgC
$M_U(t_{PI})$	1583.3 PgC
$M_D(t_{PI})$	36416.7 PgC
$M_L(t_{PI})$	2200 PgC

Table 2. Initial equilibrium pre-industrial conditions obtained for the parameters specified in Table 1.

2.4.4 Glaciers

We have fixed the total sea level rise potential of glaciers (since pre-industrial times) to 0.5m. This is an intermediate value between those reported by Levermann et al. (2013) and Farinotti et al. (2019). The sensitivity ζ has been fixed to 2 °C to mimic

Parameter	Value (s)
F_{2X}	3.9 W m^{-2}
β	1.1143 W m^{-2} °C^{-1}
γ	0.8357 W m^{-2} °C^{-1}
h_U	150 m
h_D	3000 m
c_{vol}	0.13 W yr m^{-3} °C^{-1}
α_{SO2} α_{SO_2}	65 W m^{-2}
β_{SO2} β_{SO_2}	2246 TgS yr^{-1}
γ_{SO2} γ_{SO_2}	0.23

Table 3. Values of parameters Parameter values for the temperature module.

Parameter	Value
α_U	2.3×10^{-4} °C^{-1}
α_D	1.3×10^{-4} °C^{-1}

Table 4. Thermal expansion coefficients.

the glaciers' commitment curve in (Levermann et al., 2013). Finally, the timescale has been fixed to 200 yr which corresponds to an intermediate value for the range found by Mengel et al. (2016). Figures 6 and 16 show the performance of SURFER's glaciers model against other models both on short and long timescales.

Parameter	Value
$S_{gl,pot}$	0.5 m
ζ	2 °C
τ_{gl}	200 yr

Table 5. Glacier model parameters.

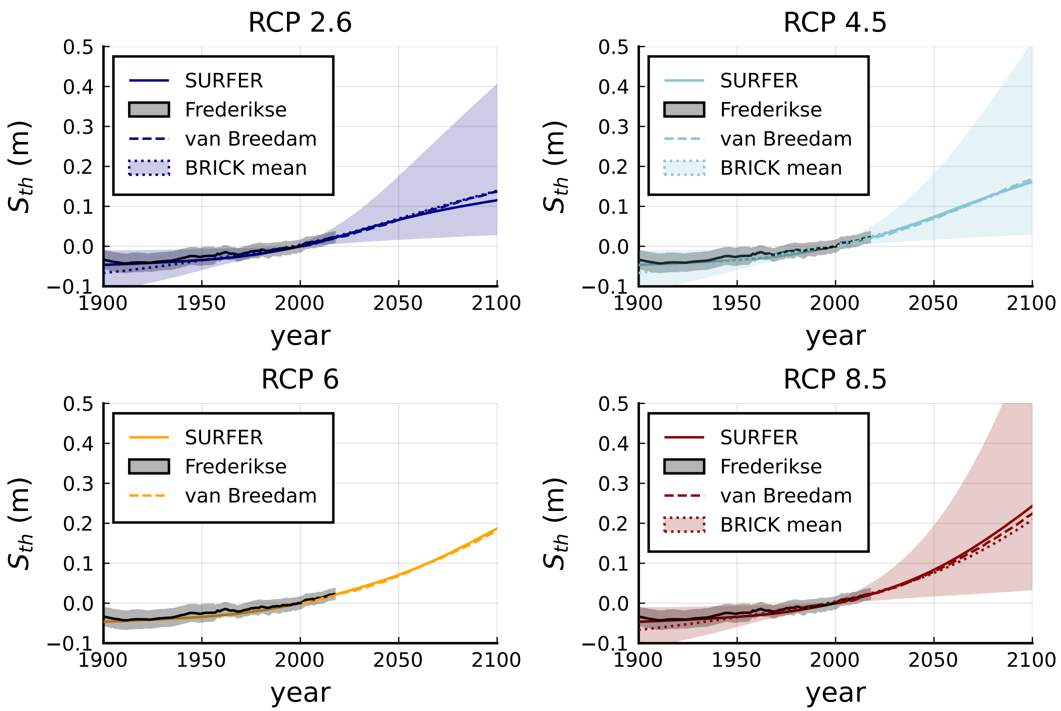

Figure 5. Sea level rise contribution from ocean thermal expansion for historical period and projections along RCP scenarios. SURFER's estimates correspond to the solid coloured lines, observations for the historical period from (Frederikse et al., 2020) are shown with solid black lines with the corresponding uncertainty range in grey shade. BRICK's mean and uncertainty range are shown with dotted lines and coloured shades. The dashed lines correspond to results of Van Breedam et al. (2020). Sea level rise is with respect to year 2000.

2.4.5 Ice sheets

We now proceed to fix the values of the parameters $(T_+, T_-, V_+, \tau_+, \tau_-)$[6] for adapting the ice sheet model to Greenland and Antarctica, see Table 6.

For Greenland, we have fixed calibrated the bifurcation points $(T_\pm, V_+)$ and by requiring the steady states of Eq. (38) to reproduce part of the steady state structure found in (Robinson et al., 2012). In Fig. 7a we show the upper and lower steady state branches found by Robinson et al. (2012) together with SURFER's double-fold steady state structure. Then, the melting timescale τ_- by fitting SURFER to the has been fixed to match the constant forcing transient results of Robinson et al. (2012)[7]; , see Fig. 7b. Finally, not many references present accumulation (ice sheet growth) experiments which are needed to fix τ_+ we have instead looked at the timescales that appear on the freezing experiments . For this reason we used different references to fix

[6]The parameter V_- has been fixed by using Eq. (40).

[7]Notice that δT_U is the global mean temperature anomaly and that their plots are for regional summer temperature anomaly. On their supplementary information they explain how to relate the two.

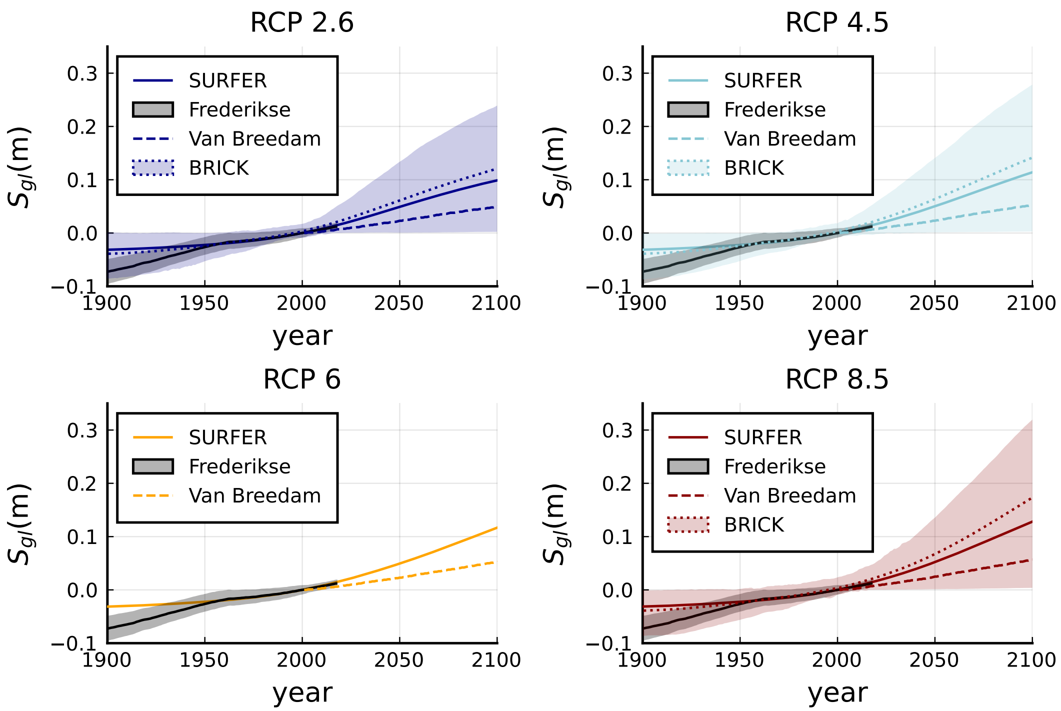

Figure 6. Sea level rise contribution from glaciers for historical period and projections along RCP scenarios. SURFER's estimates correspond to the solid coloured lines, observations for the historical period from (Frederikse et al., 2020) are shown with solid black lines with the corresponding uncertainty range in grey shade. BRICK's mean and uncertainty range are shown with dotted lines and coloured shades. The dashed lines correspond to results of Van Breedam et al. (2020). Sea level rise is with respect to year 2000.

τ_+ (Letreguilly et al., 1991; Pattyn, 2006). The calibration of τ_+ was done in the way as that of τ_-, i.e., seeking to reproduce the dynamic accumulation experiments of in (Letreguilly et al., 1991; Pattyn, 2006).

For the case of Antarctica fitting was more complicated than for Greenland. Contrary to the previous case, we are not aware of results from the same Antarctic ice sheet model setup for both steady state and transient experiments. For example, for the PISM model, Garbe et al. (2020) provided the steady state structure and Winkelmann et al. (2015) performed some transient experiments but since the climate models used for the forcing were not the same, the results are not completely compatible[8]. With this less than ideal situation, we have relied on two references, Garbe et al. (2020); Van Breedam et al. (2020)the two most recent references, (Garbe et al., 2020; Van Breedam et al., 2020), to fix SURFER's Antactica parameters $(T_\pm, V_+, \tau_-)$; the first one containing . The steady state experiments and the second one dynamical experiments . The parameter of Garbe et al. (2020) have oriented us towards the range of acceptable parameters values while we have finally fixed those values by attempting to fit the dynamical experiments of Van Breedam et al. (2020). Again, in the absence of time-series results from accumulation experiments in the same references, τ_+ has been fixed by fitting to the results of (Pattyn, 2006; Huybrechts, 1993). Bottom

[8] More melting happens in the setup of Winkelmann et al. (2015) than it would be expected by the results in (Garbe et al., 2020).

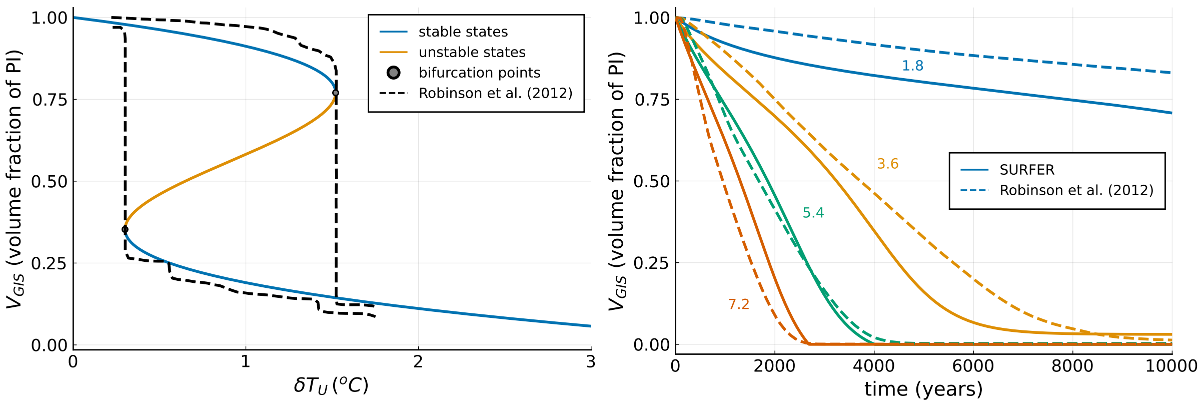

(a) Steady states

(b) Transient behaviour

Figure 7. SURFER's Greenland ice sheet against the work of Robinson et al. (2012).

left plot in Fig. 16 contrasts SURFER's prediction for S_{AIS} when forced with extended RCP scenarios to the results of Van Breedam et al. (2020).

Finally, Greenland's and ~~Antarctic~~Antarctica's ice sheet~~SLR~~ ' sea level rise potential, linking the ice volume fraction to an eustatic ~~sea-level~~ sea level rise, come from (Van Breedam et al., 2020) and (Garbe et al., 2020) respectively.

As more models provide both steady state structure and transient experiments, fitting can be improved by following the same strategy as used for Greenland. Additionally, it would be best if results from bigger models were presented separately for East and West Antarctica since the two components have different tipping points and evolve with different characteristic timescales. Then SURFER could treat East and West Antarctica as two separate ice sheets.

Again, SURFER is intended to be tuned on state-of-the art models. Its parameters can, therefore, be revised as new simulations become available. The best scenario would be to have a model inter-comparison project on the timescales of millennia for both ice sheets.

2.5 Numerics

The model has been implemented in The Julia Programming Language (Bezanson et al., 2017) in the jupyter-lab environment. The equations have been integrated using the package `DifferentialEquations.jl` with the integration method `Rosenbrock23()` with `abstol=1e-12` and `reltol=1e-3`. The model runs extremely fast, each run of up to 10000 years taking ≈ 0.003 seconds on a laptop with processor Intel® Core™ i7-9850H CPU @ 2.60GHz × 12.

3 ~~Showcasing the model~~Numerical results and comparisons

In this section we show the model's behaviour when forced by different CO_2 emission scenarios and aerosol injections. Whenever it has been possible to retrieve outputs of other models or historical data we have done so for making the ~~comparison~~

Parameter	Greenland's value	Antarctica's value
T_+	~~1.6~~ 1.52 °C	6.8 °C
T_-	~~0.4~~ 0.3 °C	~~5.5~~ 4.0 °C
V_+	0.77	~~0.55~~0.44
V_-	~~0.3649~~ 0.3527	~~0.108~~0.079
τ_+	5500 yr	5500 yr
τ_-	~~400~~ 470 yr	~~500~~ 3000 yr
~~SLR potential~~ S_{pot}	7.4 m	55 m

Table 6. ~~Values of parameters~~ Parameter values used here for Greenland and Antarctic ice sheets.

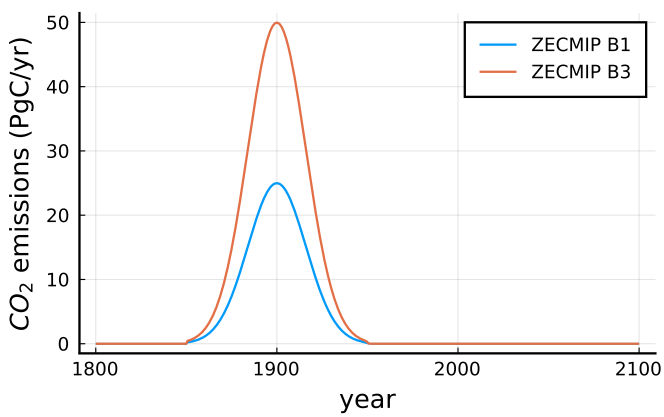

Figure 8. CO_2 emission curves for ZECMIP experiments B1 and B3.

~~easier.~~ comparisons easier. All examples start from pre-industrial conditions, more details on initial conditions can be found in Sec. 2.4.

3.1 ZECMIP B1 and B3 experiments

The Zero Emissions Commitment Model Intercomparison Project (ZECMIP) (Jones et al., 2019; MacDougall et al., 2020) was proposed to quantify the amount of unrealized temperature change that occurs after CO_2 emissions cease and to investigate the geophysical drivers behind this climate response. The ZECMIP B1 and B3 experiments ~~(Jones et al., 2019; MacDougall et al., 2020)~~ consist in starting with pre-industrial conditions and forcing the system with the bell shaped emission curves in Fig. 8, corresponding to 1000 PgC cumulated emissions for the B1 experiment and 2000 PgC for the B3 experiment. We consider the output of 6 EMICs and 2 ESMs that participated in the ZECMIP experiment. The EMICs are Bern3D-LPX-ECS3K, DCESS1.0,

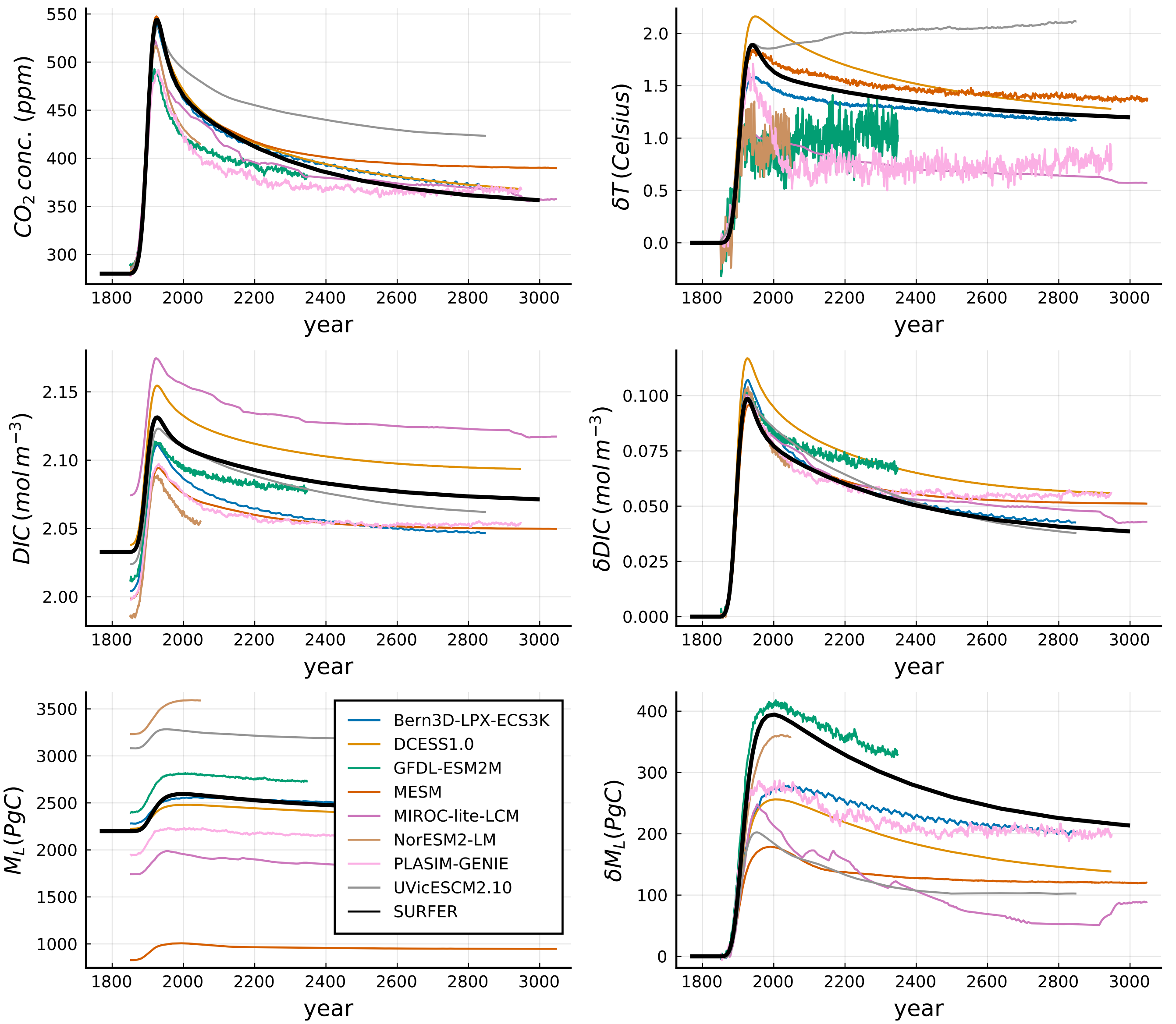

Figure 9. ZECMIP B1 experiment outputs of 6 EMICs, 2 ESMs and SURFER. From left to right, top to bottom: CO_2 concentration in the atmosphere, atmospheric global mean temperature anomaly, dissolved inorganic carbon in the upper layer, dissolved inorganic carbon anomaly in the upper layer, total of carbon in the land reservoir and carbon anomaly in land reservoir.

MESM, MIROC-lite-LCM, PLASIM-GENIE, UVicESCM2.10 and the ESMs are GFDL-ESM2M and NorESM2-LM. Figures 9 and 10 show the good agreement of SURFER's output to that of the ZECMIP experiments. SURFER's land model is closer to the ESMs than the EMICs although this can be changed by ~~tuning~~ recalibrating β_L on the carbon cycle equations.

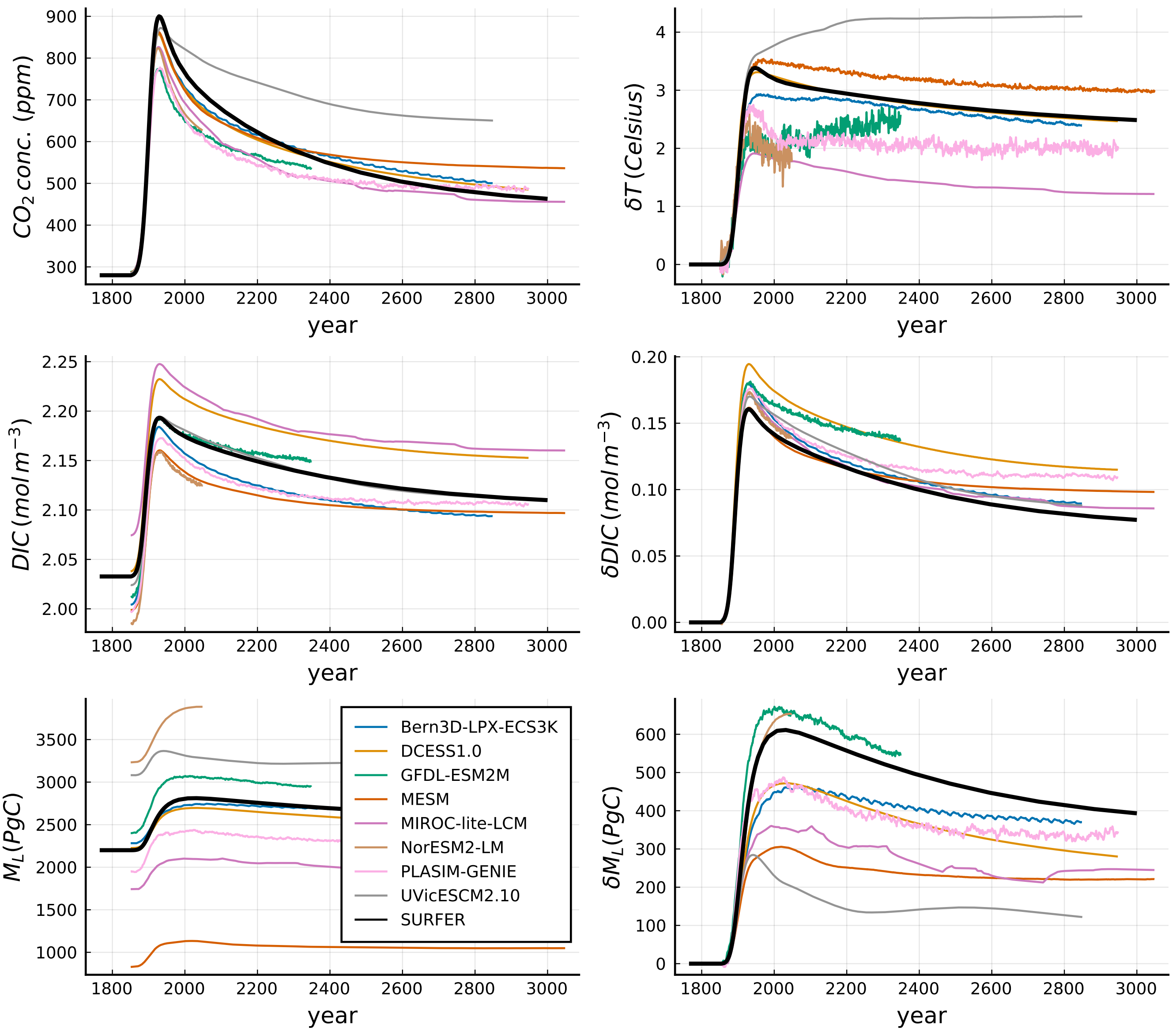

Figure 10. ZECMIP B3 experiment outputs of 6 EMICs, 2 ESMs and SURFER.. From left to right, top to bottom: CO_2 concentration in the atmosphere, atmospheric global mean temperature anomaly, dissolved inorganic carbon in the upper layer, dissolved inorganic carbon anomaly in the upper layer, total of carbon in the land reservoir and carbon anomaly in land reservoir.

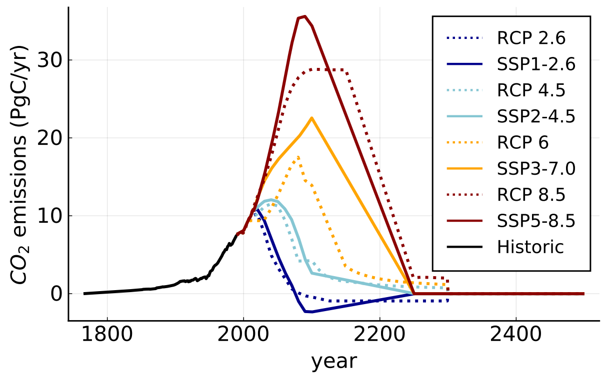

Figure 11. CO_2 emission rate for the RCP and SSP scenarios with their extensions.

3.2 Ocean acidification under RCP or SSP forcing scenarios

In this section we run SURFER forced with historic CO_2 emissions followed by CO_2 emissions associated to the Representative Concentration Pathways (RCPs) and Shared Socio-economic Pathways (SSPs) together with their extensions (Meinshausen et al., 2011, 2020)[9], see Fig. 11. For the RCPs emission scenarios we have considered, as Van Breedam et al. (2020), that CO_2 emissions are zero from 2300 onwards. For the SSPs emission scenarios, as in (Meinshausen et al., 2020), we consider that CO_2 emissions are zero from 2250. We have considered that the Solar Radiation Management sulphur injections remain zero during the whole simulation period.

Figure 12 shows the evolution of different variables when forced by these scenarios. As CO_2 is emitted into the atmosphere, the CO_2 concentration in the atmosphere rises and so does the temperature and the DIC in the ocean's upper layer. Together with the increase in DIC, the pH, carbonate concentration and aragonite saturation state decrease. For the aragonite saturation state $(\Omega_{\text{ar}})_U$, in Fig. 12, we have shadowed the region beyond the planetary boundary for ocean acidification. SURFER predicts that all considered emission scenarios cross that planetary boundary. Scenarios RCP8.5, SSP5-8.5 and SSP3-7 reach values of aragonite saturation state smaller or close to 1; in those scenarios aragonite would dissolve in the upper ocean.

Figure 13 compares SURFER's pH prediction to that of CMIP5 and CMIP6 shown in (Kwiatkowski et al., 2020). SURFER exhibits more acidification than CMIP5 and CMIP6 but it is in better agreement with CMIP6 runs.

3.3 Sea Historical sea level rise in extended RCP scenariosand centennial projections

In this section we show the long-term again run SURFER forced with historic CO_2 emissions followed by CO_2 emissions associated to the Shared Socio-economic Pathways (SSPs) together with their extensions (Meinshausen et al., 2020) up to year 2150. Solar Radiation Management sulfur injections remain zero during the whole simulation period.

[9]For the SSPs we were only able to find the emission data up to 2100. We modelled the extension with a linear function going to zero by 2250. This is what was done by Meinshausen et al. (2020) except for the lowest emission scenario SSP1-2.6.

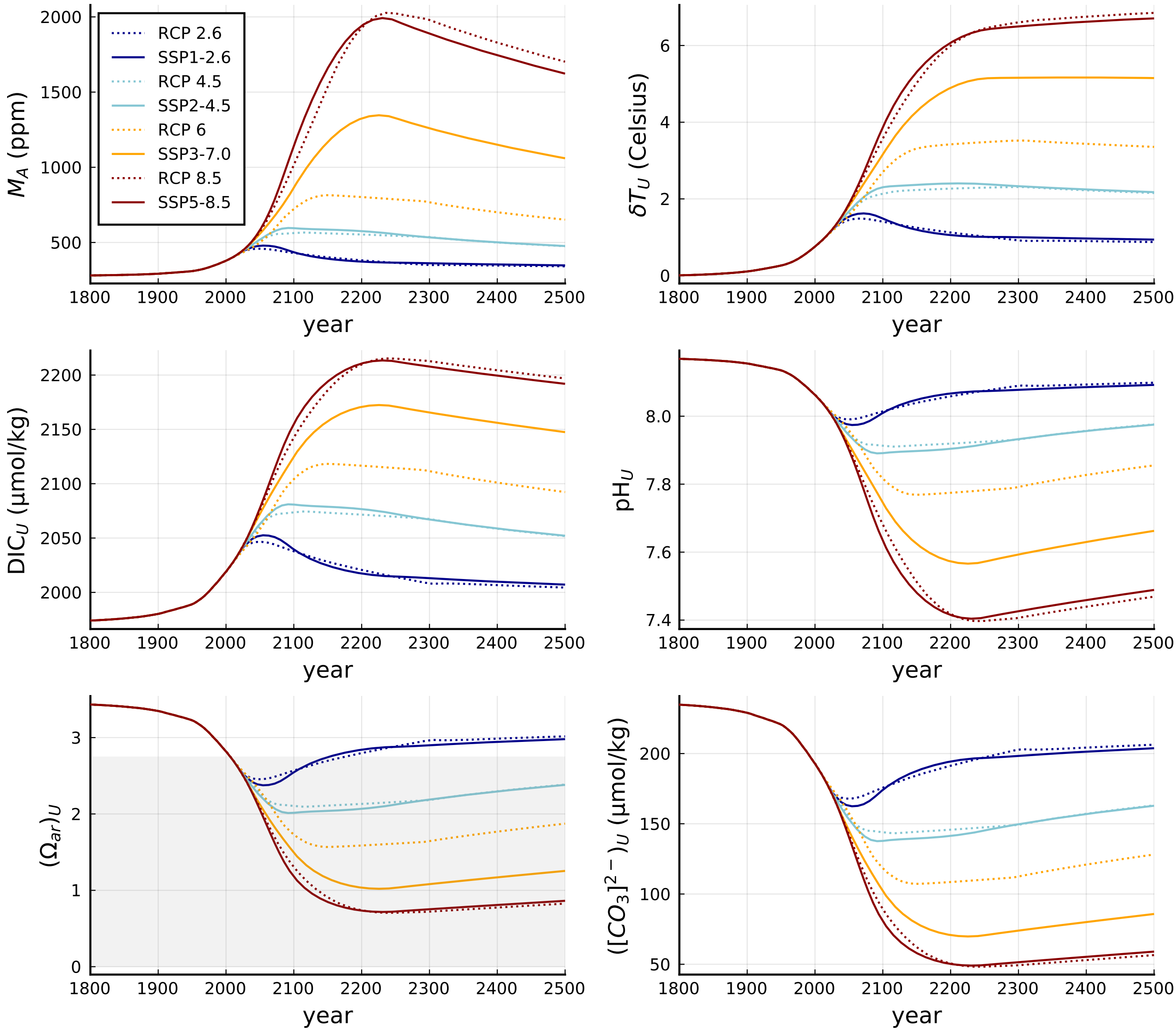

Figure 12. SURFER's output when forced by the extended RCPs and SSPs emission scenarios. From left to right, top to bottom: atmospheric CO_2 concentration, global mean temperature anomaly, Dissolved Inorganic Carbon in the upper layer, pH in the upper layer, aragonite saturation state in the upper layer and carbonate concentration in the upper layer.

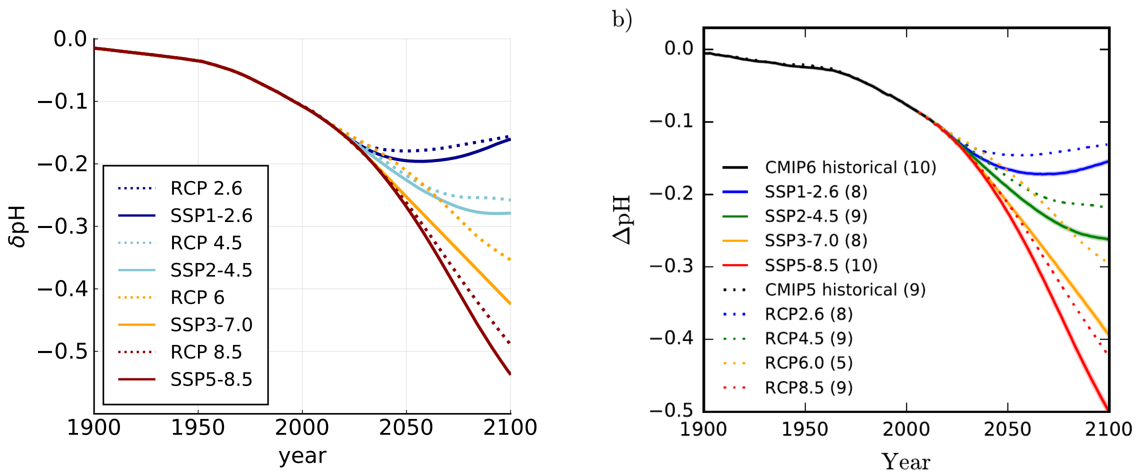

(a) SURFER (b) CMIP5 and CMIP6 results from (Kwiatkowski et al., 2020)

Figure 13. Change in pH in the upper ocean layer under RCPs and SSPs emission scenarios.

We then contrast, in Fig. 14, SURFER's sea level rise predictions to the historic observations reported in (Frederikse et al., 2020) and the projections reported in Table 9.9 of IPCC AR6 WGI, see (Fox-Kemper et al., 2021). The agreement of SURFER's predictions with both data sets is remarkable given the simplicity of the model.

3.4 Long-term (millennial) sea level rise projections

Here we show the model's long-term behaviour when forced by historic anthropogenic CO_2 emissions followed by the extended RCPs emission scenarios, see (Moss et al., 2010; Meinshausen et al., 2011), which we continue to extend from the year 2300 onwards with zero emissions, as in (Van Breedam et al., 2020), see Fig. 11.

~~Simulations were started from pre-industrial conditions considering an initial volume fraction of 1 for both ice sheets.~~ Solar Radiation Management sulfur injections remain zero during the whole simulation period.

Figure 15 shows the ~~behaviour of some of the tracked variables~~ atmospheric CO_2 concentration and the global mean temperature anomaly for a period of ~~10000 years .~~ 10,000 years and Fig. 16 contrasts SURFER's sea level rise predictions for each of the considered contributors with the corresponding results of Van Breedam et al. (2020).

Due the absence of calcium carbonate reactions in the carbon sub-model and the fact that SURFER does not include any feedback from the ice sheet melting on the temperature, quantities from the carbon cycle and climate sub-models ~~have reached~~ reach equilibrium around year ~~6000~~6,000, see Fig. 15. After that time only the ice sheet components of the model continue to evolve. If carbonate compensation was included, a slow lowering of the atmospheric CO_2 concentration and temperature would be observed, together with its corresponding effect on the ice sheets[10]. Albedo feedbacks of the ice sheets on the climate

[10] We expect this effect to be small because most of the ice sheet melting occurs in the first thousands of years where carbonate compensation still plays a very subdominant role.

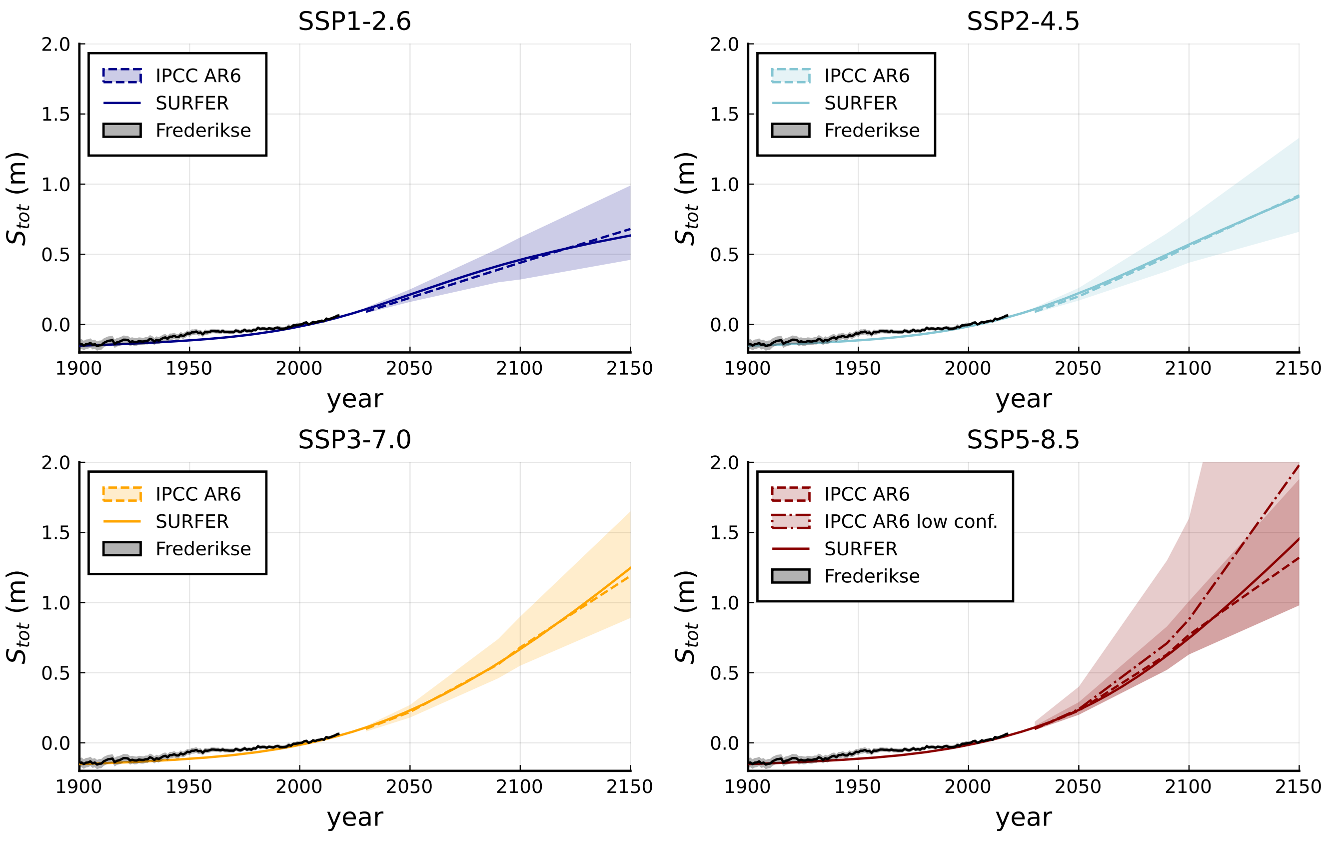

Figure 14. Historic and shorter term sea level rise projections. Solid coloured lines show SURFER's total sea level rise estimates. Solid black lines with shaded envelope correspond to historic observations reported by Frederikse et al. (2020), dashed coloured lines correspond to IPCC AR6 estimates and shaded regions to IPCC AR6 likely (medium confidence) ranges. The dash-dot line in SSP5-8.5 corresponds to the low confidence IPCC AR6 estimate. SURFER's and historical results are with respect to year 2004. IPCC results are relative to a baseline of 1995–2014.

sub-model would act in the opposite direction increasing the temperature. These effects, as mentioned in the discussion session, are expected to be relatively small.

The agreement of ~~the~~ SURFER's total sea level rise ~~plot, Fig. 15,~~ with the results ~~shown in Fig. 5 of (Van Breedam et al., 2020) is good , specially for the Antarctic ice sheet. The agreement for the Greenland's ice sheetis not as good, specially for the two lowest forcing scenarios~~of Van Breedam et al. (2020) is good for the higher emission scenarios and worse for the lower ones, see Fig. 16. The main source for the discrepancies comes, unsurprisingly, from the Greenland ice sheet' contribution. The reason for this is that we ~~fixed~~ calibrated Greenland's parameters ~~according~~ by fitting to the results of Robinson et al. (2012) and that the tipping points do not ~~exactly coincide;~~ coincide: Greenland's ice sheet in (Robinson et al., 2012), and hence SURFER's, seems to have a higher temperature tipping point than the one of in (Van Breedam et al., 2020). ~~SURFER can also track the~~

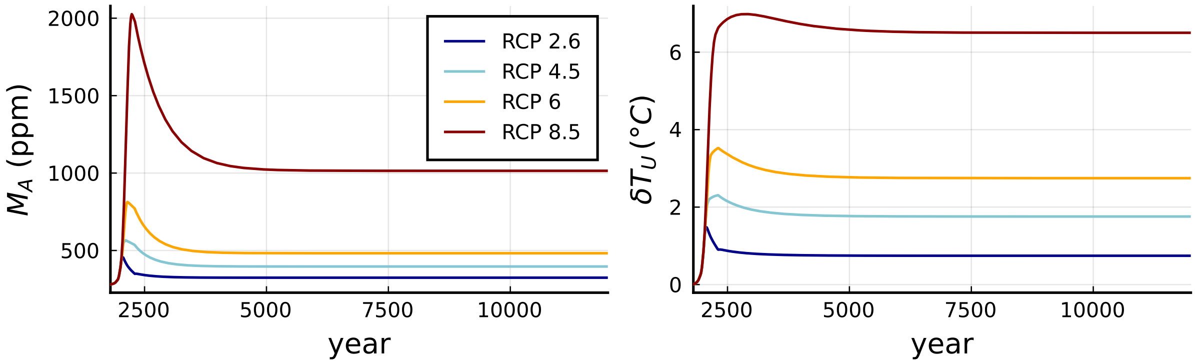

Figure 15. Long time behaviour of some of SURFER's variables when forced by RCP scenarios. From left to right, top to bottom: long-term prediction for CO_2 concentration , upper ocean and global mean temperature anomaly , cumulative sea level rise, sea level rise rate. The cumulative sea level rise plot shows contributions from Greenland and Antarctic ice sheets separately, indicated when forced by solid and dashed lines respectively. The rate of sea level rise plot shows their joint contributionextended RCP scenarios.

sea level rise rate, see Fig. 15, a quantity that plays a crucial role in the context of adaptation to sea level rise. Greenland completely melts around the year 5000 for scenario RCP-8.5, this explains the small but sharp drop in the rate of sea level rise around the same time for the corresponding scenarioThe agreement for Greenland's ice sheet with (Van Breedam et al., 2020) is therefore not good for the lower emission scenarios because the corresponding forcing temperatures lie close to this threshold in SURFER but are clearly beyond it in (Van Breedam et al., 2020).

SURFER's ocean thermal expansion parametrisation yields a S_{th} that agrees well with the results of (Van Breedam et al., 2020) , similarly for the Antarctic ice sheet. For the glaciers we have different behaviour although the same order of magnitude which, as expected, is very sub-leading with respect to the other contributors at these timescales. While for SURFER the different RCP scenarios lead to different contributions from the glaciers (higher emission scenarios leading to more melting), in (Van Breedam et al., 2020) all the considered ice in glaciers eventually melts at a rate that is scenario-dependent.

3.5 Solar radiation management

As a last example we perform an experiment done by the Geoengineering Model Inter-comparison project and compare SURFER's output to their results. We focus on the G6sulfur experiment introduced in (Kravitz et al., 2015). In the G6sulfur experiment, stratospheric aerosols are injected into the model with the goal of reducing the magnitude of the net anthropogenic radiative forcing from a high forcing scenario (SSP5-8.5) to match that of a medium forcing scenario (SSP2-4.5).

We run SURFER forced by the CO_2 emissions corresponding to the SSP scenarios SSP5-8.5 and SSP2-4.5 in the absence of solar radiation management. We compute the radiative forcing difference between the two scenarios, and we perform a third run in which SURFER is forced by the CO_2 emissions corresponding to scenario SSP5-8.5 and with sulfur aerosol injections exactly compensating the extra radiative forcing in SSP5-8.5 with respect to SSP2-4.5

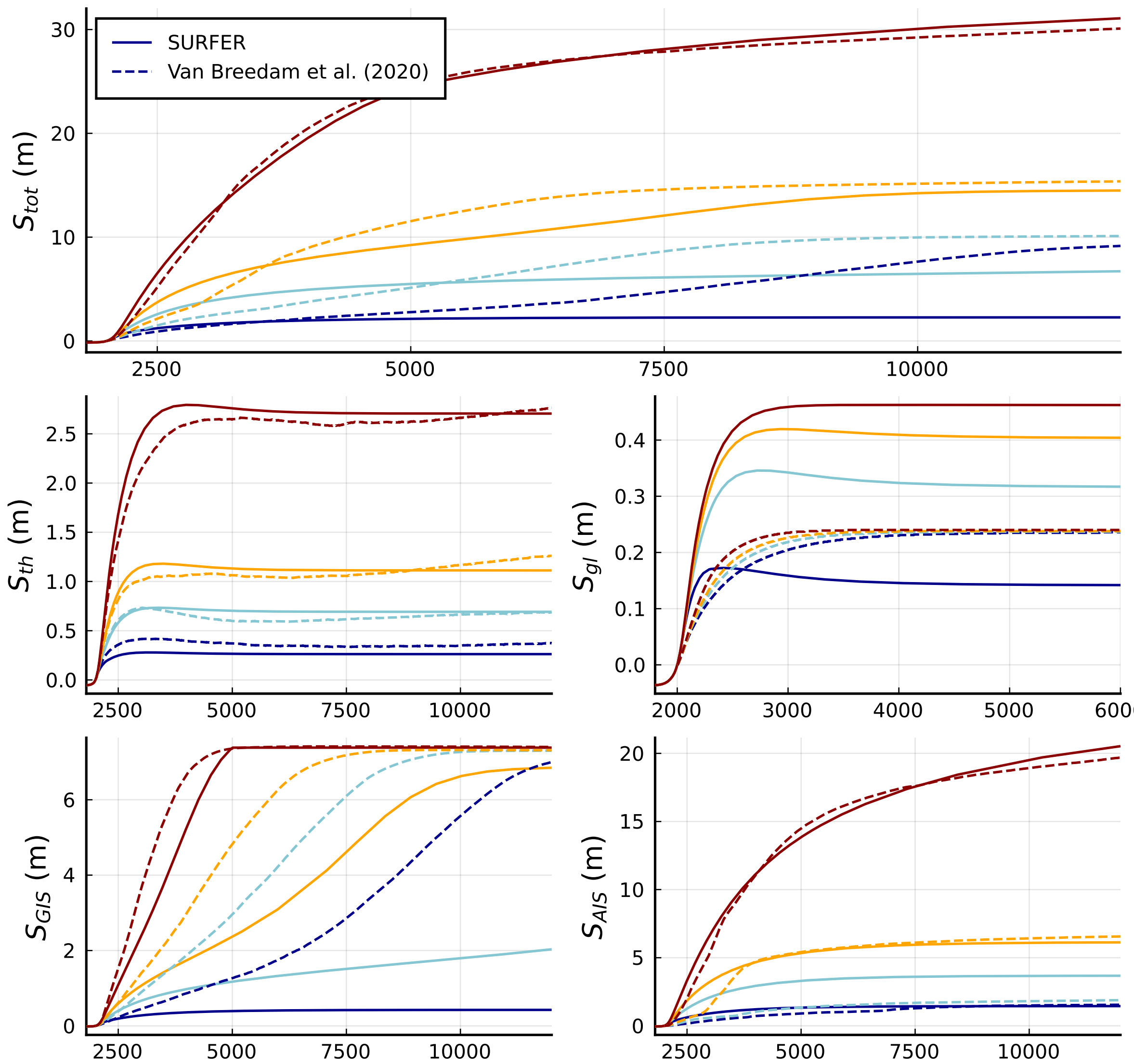

Figure 16. Long-term sea level rise from SURFER and Van Breedam et al. (2020) when forced by extended RCP scenarios. Total sea level rise and individual contributors are shown, from left to right, top to bottom: total sea level rise, ocean thermal expansion, glacier, Greenland and Antarctica contributions. Solid lines correspond to SURFER and dashed to the results in (Van Breedam et al., 2020). Colours indicate different RCP scenarios as in Fig. 15.

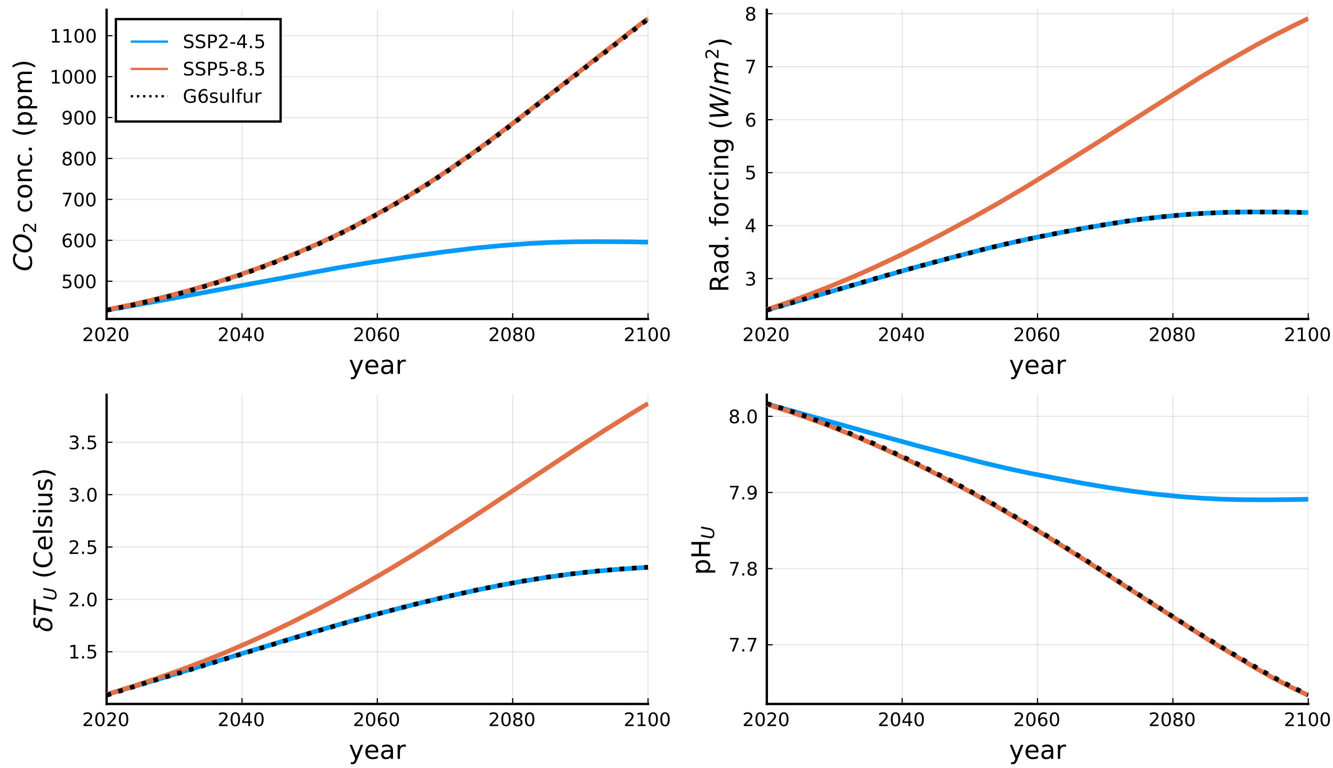

Figure 17. SURFER's output for the G6sulfur experiment. From left to right, top to bottom: CO_2 concentration, radiative forcing, temperature anomaly and pH in upper ocean layer.

$$I(t) = \beta_{SO_2}\left(-\log\left(\frac{F^{(\text{SSP5-8.5})}(t) - F^{(\text{SSP2-4.5})}(t)}{\alpha_{SO_2}}\right)\right)^{1/\gamma_{SO_2}} \tag{47}$$

with $F^{(\text{SSP2-4.5})}$ and $F^{(\text{SSP2-4.5})}$ the time varying radiative forcing obtained under the corresponding scenarios.

Figure 17 shows SURFER predictions for CO_2 concentration, radiative forcing, temperature and pH of upper ocean layer. This shows that while the radiative forcing, and hence the temperature, is lowered by the injection of aerosols, the high CO_2 concentration and ocean acidification related problems remain. In Figure is high and therefore the ocean is dangerously acidic. In Fig. 18 we compare the rate of sulfur injections needed by SURFER and by the ESMs that participated in the GeoMIP to accomplish the G6sulfur experiment.

4 Discussion

In the literature other reduced complexity models for sea level rise can be found (e.g., Wong et al., 2017; Nauels et al., 2017; Palmer et al., 2 . Wong et al. (2017) introduce BRICK, a framework for modelling sea level rise. They argue that models for risk analysis

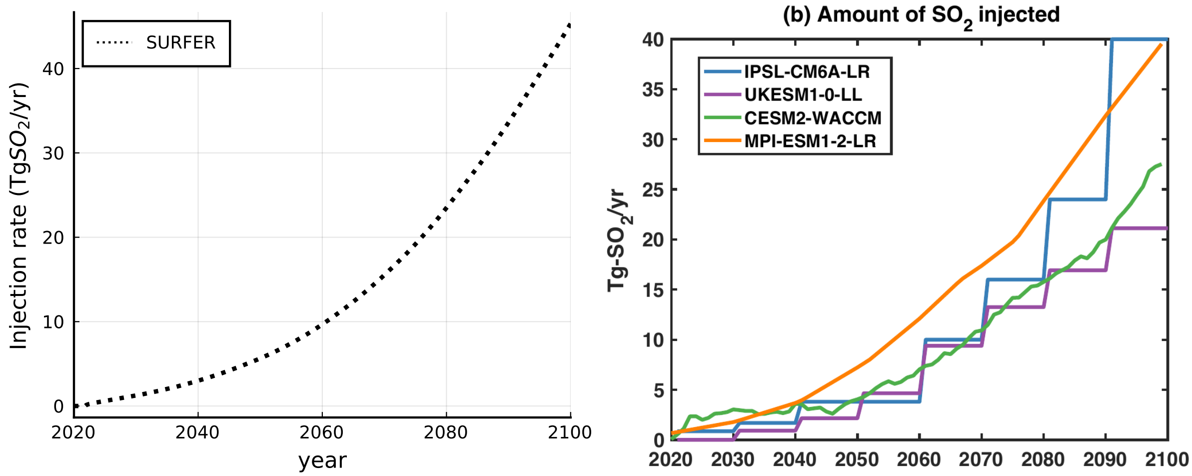

(a) SURFER G6sulfur injections

(b) GeoMIP G6sulfur injections from (Visioni et al., 2021)

Figure 18. Comparison of aerosol injection rate needed to do the G6sulfur experiment by SURFER (left) and by some ESMs participating in GeoMIP (right).

should be accessible, transparent, flexible and efficient. In this paper we have shown that SURFER complies with all of these criteria. Additionally, compared to BRICK, SURFER models ocean acidification and incorporates tipping points in the ice sheet components. Such phenomena are important when assessing policies (Lenton and Ciscar, 2013). Nauels et al. (2017) and Palmer et al. (2020) also provide efficient a reduced complexity model and a statistical emulator, respectively, that allow for sea level rise projections. These models, however, are already less transparent than SURFER and again, they do not incorporate tipping point dynamics. Finally, SURFER has been shown to reproduce results from EMICs, ESMs and 3D ice sheet models on timescales from decades to millennia. Is is unclear to us whether the BRICK, MAGICC and the model by Palmer et al. (2020) are applicable on such long timescales. Thus, we are convinced that SURFER is a valuable addition to the literature.

SURFER is simple, easy to understand and fast to run, but it misses some processes, carbon reservoirs and feedbacks. This gives room for extensions, and here we provide relevant information for users who would like to take some of the relevant processes into account, while explaining why we have not included them in the present model.

Permafrost holds approximately 1400 PgC (Canadell et al., 2021): that is about twice as much carbon as currently contained in the atmosphere. The thawing and subsequent release of part of that carbon into the atmosphere may therefore constitute a substantial positive feedback on anthropogenic emissions. Several studies, simulations and observations have been made to quantify the strength of these effects, (MacDougall and Knutti, 2016; Chadburn et al., 2017; Burke et al., 2017; Turetsky et al., 2020; Burke et al., 2020) but the spread in the estimates is considerable. MacDougall and Knutti (2016) made projections of the release of carbon from permafrost soils using a perturbed parameter ensemble with the UVic-ESCM EMIC. Among other things, they computed the sensitivities of cumulative emitted carbon per extra degree of warming. They showed the (transient) sensitivities changed with time, obtaining 24, 39, and 47 PgC/°C for the years 2100, 2200 and 2300 under all RCP scenarios.

A similar computation was done by Burke et al. (2017) with the IMOGEN model coupled to two different land models. In that case, although lower values were obtained, the sensitivities remained time dependent ($\sim$ 10, 20, 30 PgC/°C for 2100, 2200 and 2300 under all RCP scenarios). In an observation-based study, Chadburn et al. (2017) estimated an equilibrium sensitivity of permafrost area loss per degree of future global warming of $4.0^{+1.0}_{-1.1}$ million km^2/°C. The climatic consequences for CO_2 emissions from thawed permafrost were not explored. In the ZECMIP experiments (Jones et al., 2019; MacDougall et al., 2020), only two of the models (NorESM2-LM and UVicESCM2.10) had a permafrost module. The presence of the module in these models is visible on the absolute size of their land carbon reservoir compared to the other models (see Figs. 9 and 10), but not on the evolution of the land reservoir anomalies, suggesting that, in these models at least, the permafrost feedback does not dominate other carbon fluxes. Burke et al. (2020) Burke et al. (2020) acknowledges that modelling future permafrost thaw and its resulting CO_2 emissions remains a challenge to ESMs and EMICs, and points to deeper soils and the inclusion of a representation of abrupt thawing events as the main points to be improved. For this reason we left the addition of this reservoir and its possible feedbacks for the future.

The value of the equilibrium climate sensitivity used in SURFER is compatible with that obtained by ESMs that include the effect of ice-albedo feedback from the melting of sea-ice. Consequently, the ice-albedo feedback coming from sea-ice can be thought of as already included in SURFER even if sea-ice is not explicitly part of the model. A representation of the ice-albedo feedback due to the melting of the ice sheets, however, is missing in SURFER. Wunderling et al. (2020) studied the impact of the melting of several cryosphere elements on the global mean temperature. They found that the full melting of Greenland's ice sheet would lead to a temperature increase of 0.13°C. Approximately 50% of which corresponds to albedo, and the rest to changes in lapse rate, water vapour and clouds. For the west Antarctic ice sheet an increase in temperature of 0.05°C was found, again with 50% of it coming from albedo effects. The East Antarctic ice sheet was not included in the study. Adding these effects has been left for future work in which more data from geographically-explicit models becomes available.

SURFER's carbon cycle does not take into account the soft tissue or the carbonate pump which act to create a Dissolved Inorganic Carbon gradient in the water column with the deeper layer containing more DIC than the upper layer. We have introduced a constant parameter, δ_{DIC}, which allows for this difference in DIC between layers to be captured. The soft tissue and carbonate pumps might be affected by temperature and CO_2 concentration changes, leading to a time evolving δ_{DIC}, while in SURFER this parameter remains is constant.

The feedback of temperature on the physical component of the carbon cycle can be included by substituting the solubility constant K_0 and the dissociation constants K_1 and K_2 by their temperature dependent expressions as done in Glotter et al. (2014) (Glotter et al., 2014). This feedback, which acts in the direction of increasing atmospheric CO_2 by reducing the ocean carbon uptake, is however known to be small (Glotter et al., 2014) due to two competing processes; while solubility decreases with temperature, the dissociation constants increase.

Calcium carbonate compensation, a slower process in which the ocean's pH is neutralised by the dissolution of $CaCO_3$ from sediments is not present in SURFER. Calcium carbonate compensation acts on timescales of 3-7 kyr (Archer et al., 2009) and provides an extra buffer for atmospheric CO_2. Since the impact from ocean acidification on marine ecosystems takes place at much shorter timescales, and since the highest and most harmful rates of sea level rise occur before the year 4000 for the

RCP scenarios, it seems unnecessary for our purposes to add this effect (together with a sediments reservoir) into SURFER. Due to this choice its predictions will start to deviate from expected on timescales of several thousands of years and ocean acidification will be slightly intensified with respect to models which do include such processes. We have also ignored even longer timescale effects related to the CO_2 chemical reaction with silicate rocks.

In SURFER, the impact of solar radiation management with sulfur dioxide is exerted only on the globally averaged temperature. The focus on temperature may implicitly cause an under-appreciation of the risks associated with this or similar solar radiation management technologies, especially their direct impacts on atmospheric chemistry, circulation, precipitation and their indirect impacts on health and food security. As already stated in the introduction, this inclusion is motivated by the need to put in a single coherent framework the contrasting timescales of the (short) residence time of stratospheric aerosols, the (long) residence time of carbon in the ocean-atmosphere system and the timescales involved in the sea-level sea level response. We nevertheless urge potential users of SURFER interested in evaluating the cost and benefits and related dilemmas associated with solar radiation management to adequately incorporate its potentially severe adverse side effects in their studies and conclusions. Solar radiation management impacts cannot be reduced to temperature and any study considering this technology as an option should account for the multifaceted risks associated with it (Robock, 2016)(Robock, 2016, 2020). Not doing so will likely lead to bad and dangerous advice.

5 Conclusions

Most policy analyses in the context of climate change and climate policy focus on the next decades to a couple of hundreds of years. It is reasonable to ask ourselves what are the best decisions to be made in the next decades as opposed to those to be made in the next millennia. What is not reasonable is to ignore the long-term consequences of such short-term decisions in assessments. Science has shown that anthropogenic emissions have very long-term effects, not only on the temperature but also on ocean acidification and especially on sea level rise.

Moreover, they tend to focus solely on temperature , ignoring ocean acidification , In this paper we have presented SURFER, a new model that is easy to understand and modify, fast to apply, and hence well-suited to be used for policy assessment. SURFER emulates the results of EMICs and ESMs regarding CO_2 concentration, temperature anomalies, ocean acidification and sea level riseand tipping points. Here we presented SURFER, a carbon, climate, sea level rise model which is very fast and simple to use. Due . Since it emulates well a range of aggregated quantities, it can be used in policy assessments that value policies according to a wider criteria than just global mean temperature. Furthermore, due to its lightness and ability to correctly represent longer timescales, ocean acidification and millennial timescales, it is also well suited for long-sighted decision problems and for commitment and responsibility analyses in presence of uncertainty, among other kinds of policy assessments.

We have shown that SURFER's sea level rise (from module performs exceptionally well on the short timescales. Moreover, this module includes ice sheet tipping points), it is well-suited for long-sighted multi-objective policy analyses: With this model we can not only assess the short and long-term effects of anthropogenic emissions, but also put future technologies into the mix, such as carbon dioxide removal and solar radiation management.

The ice sheet part of the model , which are particularly important for good performance on the long timescales. Being parametrised on the ice sheet tipping points, the module can easily be updated to match latest research on ice sheet tipping points. In particular, one could decide to model Antarctica with two separate ice sheets, one for the West Antarctic Ice Sheet (more susceptible) andone for the East Antarctic Ice Sheet (more resilient). Likewise, the equation for the land reservoir can readily be adapted to the latest results as they become available.

SURFER is rich enough to adequately describe a number of features that should be considered when assessing the impacts of different policies and, as was shown here, itbehaves well under a big spectrum of emission scenariosin this fast growing area. With such a flexible ice sheet module, one may envision representing uncertainty about tipping behaviour as parameter uncertainty and investigating the effect of this non-deterministic setting on policy assessments.

Finally, we have shown that SURFER works well under a variety of forcing scenarios. These scenarios do not only include different rates of positive CO_2 emissions and a range of total cumulative emissions, but also future technologies such as solar radiation management and, for SSP1-2.6 and RCP2.6, carbon dioxide removal (in the form of atmospheric negative CO_2 emissions). As a consequence, SURFER is well-suited for policy assessments that require considering a variety of forcing scenarios. This is the case for sequential decision problems and also for commitment assessments that capture uncertainty about available future options regarding earth management. This last application will be the main focus of a companion paper that relies on SURFER as it's main computational engine.

Code availability. The exact version of SURFER used to produce the results used in this paper is archived on Zenodo (Martínez Montero et al., 2022) under MIT license, as is the input data to run the model and produce the plots for all the simulations presented in this paper. The data corresponding to the results of other references can be found through the corresponding cited references or by personal contact with the authors in the case of the results in (Robinson et al., 2012; Van Breedam et al., 2020).

Author contributions. Based on pertinent roles defined by CASRAI's CRediT – Contributor Roles Taxonomy: Conceptualization (MM, MC, NB, NB), Methodology (MM, MC, VC), Project Administration (MC), Software (MM), Supervision (MC), Validation (MM), Visualization (MM, NuriaB), Writing – original draft (MM), Writing – review & editing (MC, NB, NB, VC).

Competing interests. None

Acknowledgements. The authors thank the editors and reviewers, whose comments have lead to significant improvements of the original manuscript. This project is TiPES contribution #146: This project has received funding from the European Union's Horizon 2020 research and innovation programme under grant agreement No 820970". MC is funded as Research Director by the Belgian National Fund of Scientific Research. VC is funded as Research Fellow by the Belgian National Fund of Scientific Research (F.S.R.-FNRS)".

References

Archer, D.: Fate of fossil fuel CO2 in geologic time, Journal of Geophysical Research C: Oceans, 110, 1–6, https://doi.org/10.1029/2004JC002625, 2005.

Archer, D., Eby, M., Brovkin, V., Ridgwell, A., Cao, L., Mikolajewicz, U., Caldeira, K., Matsumoto, K., Munhoven, G., Montenegro, A., and Tokos, K.: Atmospheric Lifetime of Fossil Fuel Carbon Dioxide, Annual Review of Earth and Planetary Sciences, 37, 117–134, https://doi.org/10.1146/annurev.earth.031208.100206, 2009.

Arias, P.A., Bellouin, N., Coppola, E., Jones, R., Krinner, G., Marotzke, J., Naik, V., Palmer, M., Plattner, G.-K., Rogelj, J., Rojas, M., Sillmann, J., Storelvmo, T., Thorne, P., Trewin, B., Rao, K. A., Adhikary, B., Allan, R., Armour, K., Bala, G., Barimalala, R., Berger, S., Canadell, J., Cassou, C., Cherchi, A., Collins, W., Collins, W., Connors, S., Corti, S., Cruz, F., Dentener, F., Dereczynski, C., Luca, A. D., Niang, A. D., Doblas-Reyes, F., Dosio, A., Douville, H., Engelbrecht, F., Eyring, V., Fischer, E., Forster, P., Fox-Kemper, B., Fuglestvedt, J., Fyfe, J., Gillett, N., Goldfarb, L., Gorodetskaya, I., Gutierrez, J., Hamdi, R., Hawkins, E., Hewitt, H., Hope, P., Islam, A., Jones, C., Kaufman, D., Kopp, R., Kosaka, Y., Kossin, J., Krakovska, S., Lee, J.-Y., Li, J., Mauritsen, T., Maycock, T., Meinshausen, M., Min, S.-K., Monteiro, P., Ngo-Duc, T., Otto, F., Pinto, I., Pirani, A., Raghavan, K., Ranasinghe, R., Ruane, A., Ruiz, L., Sallée, J.-B., Samset, B., Sathyendranath, S., Seneviratne, S., Sörensson, A., Szopa, S., Takayabu, I., Tréguier, A.-M., van den Hurk, B., Vautard, R., von Schuckmann, K., Zaehle, S., Zhang, X., and Zickfeld, K.: 2021: Technical Summary. In Climate Change 2021: The Physical Science Basis. Contribution of Working Group I to the Sixth Assessment Report of the Intergovernmental Panel on Climate Change [Masson-Delmotte, V., P. Zhai, A. Pirani, S.L. Connors, C. Péan, S. Berger, N. Caud, Y. Chen, L. Goldfarb, M.I. Gomis, M. Huang, K. Leitzell, E. Lonnoy, J.B.R. Matthews, T.K. Maycock, T. Waterfield, O. Yelekçi, R. Yu, and B. Zhou (eds.)]. Cambridge University Press. In Press., 2021.

Bezanson, J., Edelman, A., Karpinski, S., and Shah, V. B.: Julia: A Fresh Approach to Numerical Computing, SIAM Review, 59, 65–98, https://doi.org/10.1137/141000671, 2017.

Bolin, B. and Eriksson, E.: Changes in the Carbon Dioxide Content of the Atmosphere and Sea due to Fossil Fuel Combustion, The atmosphere and the sea in motion, pp. 130–142, http://climatepositions.com/wp-content/uploads/2014/03/n8._Bolin___Eriksson__1958corrected.pdf, 1959.

Botta, N., Jansson, P., and Ionescu, C.: The impact of uncertainty on optimal emission policies, Earth System Dynamics, 9, 525–542, https://doi.org/10.5194/esd-9-525-2018, 2018.

Botta, N., Brede, N., Crucifix, M., Ionescu, C., Jansson, P., Li, Z., Martínez-Montero, M., and Richter, T.: Responsibility Under Uncertainty: Which Climate Decisions Matter Most?, Submitted to Environmental Modeling & Assessment, https://doi.org/10.21203/rs.3.rs-1103231/v1, 2021.

Burke, E. J., Ekici, A., Huang, Y., Chadburn, S. E., Huntingford, C., Ciais, P., Friedlingstein, P., Peng, S., and Krinner, G.: Quantifying uncertainties of permafrost carbon-climate feedbacks, Biogeosciences, 14, 3051–3066, https://doi.org/10.5194/bg-14-3051-2017, 2017.

Burke, E. J., Zhang, Y., and Krinner, G.: Evaluating permafrost physics in the Coupled Model Intercomparison Project 6 (CMIP6) models and their sensitivity to climate change, Cryosphere, 14, 3155–3174, https://doi.org/10.5194/tc-14-3155-2020, 2020.

Canadell, J.G., Monteiro, P. M. S., Costa, M. H., Cotrim da Cunha, L., Cox, P. M., Eliseev, A. V., Henson, S., Ishii, M., Jaccard, S., Koven, C., Lohila, A., Patra, P. K., Piao, S., Rogelj, J., Syampungani, S., Zaehle, S., and Zickfeld, K.: 2021: Global Carbon and other Biogeochemical Cycles and Feedbacks. In Climate Change 2021: The Physical Science Basis. Contribution of Working Group I to the Sixth Assessment Report of the Intergovernmental Panel on Climate Change [Masson-Delmotte, V., P. Zhai, A. Pirani, S.L. Connors, C. Péan, S. Berger, N.

Caud, Y. Chen, L. Goldfarb, M.I. Gomis, M. Huang, K. Leitzell, E. Lonnoy, J.B.R. Matthews, T.K. Maycock, T. Waterfield, O. Yelekçi, R. Yu, and B. Zhou (eds.)]. Cambridge University Press. In Press., 2021.

Carlino, A., Giuliani, M., Tavoni, M., and Castelletti, A.: Multi-objective optimal control of a simple stochastic climate-economy model, IFAC-PapersOnLine, 53, 16 593–16 598, https://doi.org/10.1016/j.ifacol.2020.12.786, 2020.

Chadburn, S. E., Burke, E. J., Cox, P. M., Friedlingstein, P., Hugelius, G., and Westermann, S.: An observation-based constraint on permafrost loss as a function of global warming, Nature Climate Change, 7, 340–344, https://doi.org/10.1038/nclimate3262, 2017.

Clark, P. U., Shakun, J. D., Marcott, S. A., Mix, A. C., Eby, M., Kulp, S., Levermann, A., Milne, G. A., Pfister, P. L., Santer, B. D., Schrag, D. P., Solomon, S., Stocker, T. F., Strauss, B. H., Weaver, A. J., Winkelmann, R., Archer, D., Bard, E., Goldner, A., Lambeck, K., Pierrehumbert, R. T., and Plattner, G. K.: Consequences of twenty-first-century policy for multi-millennial climate and sea-level change, Nature Climate Change, 6, 360–369, https://doi.org/10.1038/nclimate2923, 2016.

Farinotti, D., Huss, M., Fürst, J. J., Landmann, J., Machguth, H., Maussion, F., and Pandit, A.: A consensus estimate for the ice thickness distribution of all glaciers on Earth, Nature Geoscience, 12, 168–173, https://doi.org/10.1038/s41561-019-0300-3, 2019.

Fox-Kemper, B., Hewitt, H., Xiao, C., Aðalgeirsdóttir, G., Drijfhout, S., Edwards, T., Golledge, N., Hemer, M., Kopp, R., Krinner, G., Mix, A., Notz, D., Nowicki, S., Nurhati, I., Ruiz, L., Sallée, J.-B., Slangen, A., and Yu, Y.: Ocean, Cryosphere and Sea Level Change, p. 1211–1362, Cambridge University Press, Cambridge, United Kingdom and New York, NY, USA, https://doi.org/10.1017/9781009157896.011, 2021.

Frederikse, T., Landerer, F., Caron, L., Adhikari, S., Parkes, D., Humphrey, V. W., Dangendorf, S., Hogarth, P., Zanna, L., Cheng, L., and Wu, Y. H.: The causes of sea-level rise since 1900, Nature, 584, 393–397, https://doi.org/10.1038/s41586-020-2591-3, 2020.

Garbe, J., Albrecht, T., Levermann, A., Donges, J. F., and Winkelmann, R.: The hysteresis of the Antarctic Ice Sheet, Nature, 585, 538–544, https://doi.org/10.1038/s41586-020-2727-5, 2020.

Gardiner, S. M.: Is "Arming the Future" with Geoengineering Really the Lesser Evil? Some doubts about the ethics of intentionally manipulating the climate system. In Climate Ethics: Essential Readings, https://doi.org/10.1093/oso/9780195399622.001.0001, 2010.

Glotter, M. J., Pierrehumbert, R. T., Elliott, J. W., Matteson, N. J., and Moyer, E. J.: A simple carbon cycle representation for economic and policy analyses, Climatic Change, 126, 319–335, https://doi.org/10.1007/s10584-014-1224-y, 2014.

Gregory, J., George, S., and Smith, R.: Large and irreversible future decline of the Greenland ice-sheet, The Cryosphere Discussions, pp. 1–28, https://doi.org/10.5194/tc-2020-89, 2020.

Gregory, J. M.: Vertical heat transports in the ocean and their effect on time-dependent climate change, Climate Dynamics, 16, 501–515, https://doi.org/10.1007/s003820000059, 2000.

Gutiérrez, J.M., Jones, R., Narisma, G., Alves, L., Amjad, M., Gorodetskaya, I., Grose, M., Klutse, N., Krakovska, S., Li, J., Martínez-Castro, D., Mearns, L., Mernild, S., Ngo-Duc, T., van den Hurk, B., , and Yoon, J.-H.: 2021: Atlas. In Climate Change 2021: The Physical Science Basis. Contribution of Working Group I to the Sixth Assessment Report of the Intergovernmental Panel on Climate Change [Masson-Delmotte, V., P. Zhai, A. Pirani, S.L. Connors, C. Péan, S. Berger, N. Caud, Y. Chen, L. Goldfarb, M.I. Gomis, M. Huang, K. Leitzell, E. Lonnoy, J.B.R. Matthews, T.K. Maycock, T. Waterfield, O. Yelekçi, R. Yu, and B. Zhou (eds.)]., 2021.

Hänsel, M. C., Drupp, M. A., Johansson, D. J., Nesje, F., Azar, C., Freeman, M. C., Groom, B., and Sterner, T.: Climate economics support for the UN climate targets, Nature Climate Change, 10, 781–789, https://doi.org/10.1038/s41558-020-0833-x, 2020.

Heitzig, J., Kittel, T., Donges, J. F., and Molkenthin, N.: Topology of sustainable management of dynamical systems with desirable states: from defining planetary boundaries to safe operating spaces in the Earth system, Earth System Dynamics, 7, 21–50, https://doi.org/10.5194/esd-7-21-2016, 2016.

Held, I. M., Winton, M., Takahashi, K., Delworth, T., Zeng, F., and Vallis, G. K.: Probing the fast and slow components of global warming by returning abruptly to preindustrial forcing, Journal of Climate, 23, 2418–2427, https://doi.org/10.1175/2009JCLI3466.1, 2010.

Helwegen, K. G., Wieners, C. E., Frank, J. E., and Dijkstra, H. A.: Complementing CO2 emission reduction by solar radiation management might strongly enhance future welfare, Earth System Dynamics, 10, 453–472, https://doi.org/10.5194/esd-10-453-2019, 2019.

Huybrechts, P.: Glaciological Modelling of the Late Cenozoic East Antarctic Ice Sheet: Stability or Dynamism?, Geografiska Annaler: Series A, Physical Geography, 75, 221–238, https://doi.org/10.1080/04353676.1993.11880395, 1993.

Jones, C. D., Frölicher, T. L., Koven, C., MacDougall, A. H., Damon Matthews, H., Zickfeld, K., Rogelj, J., Tokarska, K. B., Gillett, N. P., Ilyina, T., Meinshausen, M., Mengis, N., Séférian, R., Eby, M., and Burger, F. A.: The Zero Emissions Commitment Model Intercomparison Project (ZECMIP) contribution to C4MIP: Quantifying committed climate changes following zero carbon emissions, Geoscientific Model Development, 12, 4375–4385, https://doi.org/10.5194/gmd-12-4375-2019, 2019.

Keen, S.: The appallingly bad neoclassical economics of climate change, Globalizations, pp. 1–33, https://doi.org/10.1080/14747731.2020.1807856, 2020.

Keen, S., Lenton, T. M., Godin, A., Yilmaz, D., Grasselli, M., and Garrett, T. J.: Economists' erroneous estimates of damages from climate change, http://arxiv.org/abs/2108.07847, 2021.

Kravitz, B., Robock, A., Tilmes, S., Boucher, O., English, J. M., Irvine, P. J., Jones, A., Lawrence, M. G., MacCracken, M., Muri, H., Moore, J. C., Niemeier, U., Phipps, S. J., Sillmann, J., Storelvmo, T., Wang, H., and Watanabe, S.: The Geoengineering Model Intercomparison Project Phase 6 (GeoMIP6): Simulation design and preliminary results, Geoscientific Model Development, 8, 3379–3392, https://doi.org/10.5194/gmd-8-3379-2015, 2015.

Kwiatkowski, L., Torres, O., Bopp, L., Aumont, O., Chamberlain, M., Christian, J., Dunne, J., Gehlen, M., Ilyina, T., John, J., Lenton, A., Li, H., Lovenduski, N., Orr, J., Palmieri, J., Schwinger, J., Séférian, R., Stock, C., Tagliabue, A., Takano, Y., Tjiputra, J., Toyama, K., Tsujino, H., Watanabe, M., Yamamoto, A., Yool, A., and Ziehn, T.: Twenty-first century ocean warming, acidification, deoxygenation, and upper ocean nutrient decline from CMIP6 model projections, Biogeosciences Discussions, pp. 1–43, https://doi.org/10.5194/bg-2020-16, 2020.

Lenton, T. M. and Ciscar, J. C.: Integrating tipping points into climate impact assessments, Climatic Change, 117, 585–597, https://doi.org/10.1007/s10584-012-0572-8, 2013.

Lenton, T. M., Held, H., Kriegler, E., Hall, J. W., Lucht, W., Rahmstorf, S., and Schellnhuber, H. J.: Tipping elements in the Earth's climate system, Proceedings of the National Academy of Sciences, 105, 1786–1793, https://doi.org/10.1073/pnas.0705414105, 2008.

Letreguilly, A., Huybrechts, P., and Reeh, N.: Steady-state characteristics of the Greenland ice sheet under different climates, Journal of Glaciology, 37, 149–157, https://doi.org/10.1017/S0022143000042908, 1991.

Levermann, A., Clark, P. U., Marzeion, B., Milne, G. A., Pollard, D., Radic, V., and Robinson, A.: The multimillennial sea-level commitment of global warming, Proceedings of the National Academy of Sciences of the United States of America, 110, 13 745–13 750, https://doi.org/10.1073/pnas.1219414110, 2013.

MacDougall, A. H. and Knutti, R.: Projecting the release of carbon from permafrost soils using a perturbed parameter ensemble modelling approach, Biogeosciences, 13, 2123–2136, https://doi.org/10.5194/bg-13-2123-2016, 2016.

MacDougall, A. H., Frölicher, T. L., Jones, C. D., Rogelj, J., DamonMatthews, H., Zickfeld, K., Arora, V. K., Barrett, N. J., Brovkin, V., Burger, F. A., Eby, M., Eliseev, A. V., Hajima, T., Holden, P. B., Jeltsch-Thömmes, A., Koven, C., Mengis, N., Menviel, L., Michou, M., Mokhov, I. I., Oka, A., Schwinger, J., Séférian, R., Shaffer, G., Sokolov, A., Tachiiri, K., Tjiputra, J., Wiltshire, A., and Ziehn, T.: Is there warming in the pipeline? A multi-model analysis of the Zero Emissions Commitment from CO2, Biogeosciences, 17, 2987–3016, https://doi.org/10.5194/bg-17-2987-2020, 2020.

Martínez Montero, M., Crucifix, M., Brede, N., and Botta, N.: Commitment as lost opportunities, in: EGU General Assembly 2022, Vienna, Austria, 23–27 May 2022, EGU22-5928, https://doi.org/https://doi.org/10.5194/egusphere-egu22-5928, 2022.

Martínez Montero, M., Crucifix, M., Couplet, V., Brede, N., and Botta, N.: SURFER v2.0.0, https://doi.org/10.5281/zenodo.6938017, 2022.

Meinshausen, M., Smith, S. J., Calvin, K., Daniel, J. S., Kainuma, M. L., Lamarque, J., Matsumoto, K., Montzka, S. A., Raper, S. C., Riahi, K., Thomson, A., Velders, G. J., and van Vuuren, D. P.: The RCP greenhouse gas concentrations and their extensions from 1765 to 2300, Climatic Change, 109, 213–241, https://doi.org/10.1007/s10584-011-0156-z, 2011.

Meinshausen, M., Nicholls, Z. R. J., Lewis, J., Gidden, M. J., Vogel, E., Freund, M., Beyerle, U., Gessner, C., Nauels, A., Bauer, N., Canadell, J. G., Daniel, J. S., John, A., Krummel, P. B., Luderer, G., Meinshausen, N., Montzka, S. A., Rayner, P. J., Reimann, S., Smith, S. J., van den Berg, M., Velders, G. J. M., Vollmer, M. K., and Wang, R. H. J.: The shared socio-economic pathway (SSP) greenhouse gas concentrations and their extensions to 2500, Geoscientific Model Development, 13, 3571–3605, https://doi.org/10.5194/gmd-13-3571-2020, 2020.

Mengel, M., Levermann, A., Frieler, K., Robinson, A., Marzeion, B., and Winkelmann, R.: Future sea level rise constrained by observations and long-term commitment, Proceedings of the National Academy of Sciences of the United States of America, 113, 2597–2602, https://doi.org/10.1073/pnas.1500515113, 2016.

Mengel, M., Nauels, A., Rogelj, J., and Schleussner, C. F.: Committed sea-level rise under the Paris Agreement and the legacy of delayed mitigation action, Nature Communications, 9, 1–10, https://doi.org/10.1038/s41467-018-02985-8, 2018.

Moreno-Cruz, J. B. and Keith, D. W.: Climate policy under uncertainty: A case for solar geoengineering, Climatic Change, 121, 431–444, https://doi.org/10.1007/s10584-012-0487-4, 2013.

Moss, R. H., Edmonds, J. A., Hibbard, K. A., Manning, M. R., Rose, S. K., Van Vuuren, D. P., Carter, T. R., Emori, S., Kainuma, M., Kram, T., Meehl, G. A., Mitchell, J. F., Nakicenovic, N., Riahi, K., Smith, S. J., Stouffer, R. J., Thomson, A. M., Weyant, J. P., and Wilbanks, T. J.: The next generation of scenarios for climate change research and assessment, Nature, 463, 747–756, https://doi.org/10.1038/nature08823, 2010.

Nauels, A., Meinshausen, M., Mengel, M., Lorbacher, K., and Wigley, T. M.: Synthesizing long-Term sea level rise projections-The MAGICC sea level model v2.0, Geoscientific Model Development, 10, 2495–2524, https://doi.org/10.5194/gmd-10-2495-2017, 2017.

Nauels, A., Gütschow, J., Mengel, M., Meinshausen, M., Clark, P. U., and Schleussner, C. F.: Attributing long-term sea-level rise to Paris Agreement emission pledges, Proceedings of the National Academy of Sciences of the United States of America, 116, 23 487–23 492, https://doi.org/10.1073/pnas.1907461116, 2019.

Niemeier, U. and Timmreck, C.: What is the limit of climate engineering by stratospheric injection of SO2?, Atmospheric Chemistry and Physics, 15, 9129–9141, https://doi.org/10.5194/acp-15-9129-2015, 2015.

Nordhaus, W. D.: The 'DICE' Model: Background and Structure of a Dynamic Integrated Climate-Economy Model of the Economics of Global Warming, http://ideas.repec.org/p/cwl/cwldpp/1009.html, 1992.

Nordhaus, W. D.: DICE 2013R: Introduction and User's Manual, Yale University Press, p. 102, http://www.econ.yale.edu/$\sim$nordhaus/homepage/homepage/documents/DICE_Manual_100413r1.pdf, 2013.

Palmer, M. D., Gregory, J. M., Bagge, M., Calvert, D., Hagedoorn, J. M., Howard, T., Klemann, V., Lowe, J. A., Roberts, C. D., Slangen, A. B., and Spada, G.: Exploring the Drivers of Global and Local Sea-Level Change Over the 21st Century and Beyond, Earth's Future, 8, https://doi.org/10.1029/2019EF001413, 2020.

Pattyn, F.: GRANTISM: An Excel™ model for Greenland and Antarctic ice-sheet response to climate changes, Computers and Geosciences, 32, 316–325, https://doi.org/10.1016/j.cageo.2005.06.020, 2006.

Ridley, J., Gregory, J. M., Huybrechts, P., and Lowe, J.: Thresholds for irreversible decline of the Greenland ice sheet, Climate Dynamics, 35, 1065–1073, https://doi.org/10.1007/s00382-009-0646-0, 2010.

Robinson, A., Calov, R., and Ganopolski, A.: Multistability and critical thresholds of the Greenland ice sheet, Nature Climate Change, 2, 429–432, https://doi.org/10.1038/nclimate1449, 2012.

Robock, A.: Albedo enhancement by stratospheric sulfur injections: More research needed, Earth's Future, 4, 644–648, https://doi.org/10.1002/2016EF000407, 2016.

Robock, A.: Benefits and risks of stratospheric solar radiation management for climate intervention (Geoengineering), Bridge, 50, 59–67, funding Information: This work has been supported by NSF grant AGS-1617844. Available at http://climate.envsci.rutgers.edu/pdf/RobockBridge.pdf, 2020.

Rockström, J., Steffen, W., Noone, K., Persson, Å., Chapin, F. S., Lambin, E. F., Lenton, T. M., Scheffer, M., Folke, C., Schellnhuber, H. J., Nykvist, B., de Wit, C. A., Hughes, T., van der Leeuw, S., Rodhe, H., Sörlin, S., Snyder, P. K., Costanza, R., Svedin, U., Falkenmark, M., Karlberg, L., Corell, R. W., Fabry, V. J., Hansen, J., Walker, B., Liverman, D., Richardson, K., Crutzen, P., and Foley, J. A.: A safe operating space for humanity, Nature, 461, 472–475, https://doi.org/10.1038/461472a, 2009.

Sarmiento, J. and Gruber, N.: Ocean Biogeochemical Dynamics, Princeton University Press, https://press.princeton.edu/books/hardcover/9780691017075/ocean-biogeochemical-dynamics, 2006.

Shepherd, T. G.: Storyline approach to the construction of regional climate change information, Proceedings of the Royal Society A: Mathematical, Physical and Engineering Sciences, 475, https://doi.org/10.1098/rspa.2019.0013, 2019.

Shepherd, T. G., Boyd, E., Calel, R. A., Chapman, S. C., Dessai, S., Dima-West, I. M., Fowler, H. J., James, R., Maraun, D., Martius, O., Senior, C. A., Sobel, A. H., Stainforth, D. A., Tett, S. F., Trenberth, K. E., van den Hurk, B. J., Watkins, N. W., Wilby, R. L., and Zenghelis, D. A.: Storylines: an alternative approach to representing uncertainty in physical aspects of climate change, Climatic Change, 151, 555–571, https://doi.org/10.1007/s10584-018-2317-9, 2018.

Steffen, W., Richardson, K., Rockstrom, J., Cornell, S. E., Fetzer, I., Bennett, E. M., Biggs, R., Carpenter, S. R., de Vries, W., de Wit, C. A., Folke, C., Gerten, D., Heinke, J., Mace, G. M., Persson, L. M., Ramanathan, V., Reyers, B., and Sorlin, S.: Planetary boundaries: Guiding human development on a changing planet, Science, 347, 1259 855–1259 855, https://doi.org/10.1126/science.1259855, 2015.

Turetsky, M. R., Abbott, B. W., Jones, M. C., Anthony, K. W., Olefeldt, D., Schuur, E. A., Grosse, G., Kuhry, P., Hugelius, G., Koven, C., Lawrence, D. M., Gibson, C., Sannel, A. B. K., and McGuire, A. D.: Carbon release through abrupt permafrost thaw, Nature Geoscience, 13, 138–143, https://doi.org/10.1038/s41561-019-0526-0, 2020.

Van Breedam, J., Goelzer, H., and Huybrechts, P.: Semi-equilibrated global sea-level change projections for the next 10 000 years, Earth System Dynamics, 11, 953–976, https://doi.org/10.5194/esd-11-953-2020, 2020.

Visioni, D., MacMartin, D., Kravitz, B., Boucher, O., Jones, A., Lurton, T., Martine, M., Mills, M., Nabat, P., Niemeier, U., Séférian, R., and Tilmes, S.: Identifying the sources of uncertainty in climate model simulations of solar radiation modification with the G6sulfur and G6solar Geoengineering Model Intercomparison Project (GeoMIP) simulations, Atmospheric Chemistry and Physics, pp. 1–37, https://doi.org/10.5194/acp-2021-133, 2021.

Williams, R. G., Goodwin, P., Ridgwell, A., and Woodworth, P. L.: How warming and steric sea level rise relate to cumulative carbon emissions, Geophysical Research Letters, 39, 4–9, https://doi.org/10.1029/2012GL052771, 2012.

Winkelmann, R., Levermann, A., Ridgwell, A., and Caldeira, K.: Combustion of available fossil fuel resources sufficient to eliminate the Antarctic Ice Sheet, Science Advances, 1, 1–6, https://doi.org/10.1126/sciadv.1500589, 2015.

Wong, T. E., Bakker, A. M. R., Ruckert, K., Applegate, P., Slangen, A. B. A., and Keller, K.: BRICK v0.2, a simple, accessible, and transparent model framework for climate and regional sea-level projections, Geoscientific Model Development, 10, 2741–2760, https://doi.org/10.5194/gmd-10-2741-2017, 2017.

Wunderling, N., Willeit, M., Donges, J. F., and Winkelmann, R.: Global warming due to loss of large ice masses and Arctic summer sea ice, Nature Communications, 11, 1–8, https://doi.org/10.1038/s41467-020-18934-3, 2020.